Tetrameric UvrD helicase is located at the *E. coli* replisome due to frequent replication blocks

Adam J. M Wollman[1,2,3,], Aisha H. Syeda[1,2,] Jamieson A. L. Howard[1,2], Alex Payne-Dwyer[1,2], Andrew Leech[4], Dominika Warecka[2], Colin Guy[5, 6], Peter McGlynn[2,6], Michelle Hawkins[2] and Mark C. Leake[1,2]

The authors wish it to be known that, in their opinion, the first two authors should be regarded as joint First Authors

[1] School of Physics, Engineering and Technology, University of York, York YO10 5DD, United Kingdom.

[2] Department of Biology, University of York, York YO10 5DD, United Kingdom.

[3] Current address: Biosciences Institute, Newcastle University, NE1 7RU, United Kingdom.

[4] Bioscience Technology Facility, Department of Biology, University of York, York YO10 5DD, United Kingdom

[5] Current address: Covance Laboratories Ltd., Otley Road, Harrogate, HG3 1PY, United Kingdom

[6] Previous address: School of Medical Sciences, Institute of Medical Sciences, University of Aberdeen, Foresterhill, Aberdeen AB25 2ZD, United Kingdom

* To whom correspondence should be addressed. To whom correspondence should be addressed. Tel: +44 (0)1904322697. Email: mark.leake@york.ac.uk

Present Address: School of Physics, Engineering and Technology, and Department of Biology, University of York, York YO10 5DD, United Kingdom

SUMMARY

DNA replication in all organisms must overcome nucleoprotein blocks to complete genome duplication. Accessory replicative helicases in *Escherichia coli*, Rep and UvrD, help remove these blocks and aid the re-initiation of replication. Mechanistic details of Rep function have emerged from recent live cell studies; however, the division of UvrD functions between its activities in DNA repair and role as an accessory helicase remain unclear in live cells. By integrating super-resolved single-molecule fluorescence microscopy with biochemical analysis, we find that UvrD self-associates into tetrameric assemblies and, unlike Rep, is not recruited to a specific replisome protein despite being found at approximately 80% of replication forks. Instead, its colocation with forks is likely due to the very high frequency of replication blocks composed of DNA-bound proteins, including RNA polymerase and factors involved in repairing DNA damage. Deleting *rep* and DNA repair factor genes *mutS* and *uvrA*, and inhibiting transcription through RNA polymerase mutation and antibiotic inhibition,

indicates that the level of UvrD at the fork is dependent on UvrD's function. Our findings show that UvrD is recruited to sites of nucleoprotein blocks via different mechanisms to Rep and plays a multi-faceted role in ensuring successful DNA replication.

INTRODUCTION

Replication and transcription of DNA occur simultaneously in *Escherichia coli,* making conflicts between the bacterial replisome, the molecular replication machine comprising in excess of 10 different proteins, and RNA polymerase (RNAP) inevitable (1–4). Collisions between replication and transcription machineries hinder replication fork progression and cause genome instability (5–14). RNAP can pause, stall and backtrack while actively transcribing, and any immobile RNAP presents long-lived barriers to replisomes (15, 16); RNAP is the most common nucleoprotein obstacle for translocating replisomes. DNA is also frequently damaged in normal growth conditions due to exposure to endogenous and exogenous DNA damaging agents, which also presents significant obstacles for replication (17–19).

Several mechanisms exist to reduce conflict between the replisome and nucleoprotein blocks. For example, transcription elongation and termination factors reduce the number of immobile RNAPs on DNA (1, 18, 20–24). Head-on collisions were originally thought to be more harmful (25–27) and therefore more important to resolve; a view supported by the occurrence of highly transcribed genes encoded on the leading strand, presumably to ensure co-directional transcription and replication (26, 28, 29). However, co-directional collisions of the replisome and RNAP also impact fork progression (3, 18, 30).

Accessory replicative helicases, identified in prokaryotes and eukaryotes, promote fork movement through resolving nucleoprotein blocks (1, 12, 13, 31, 32). The Rep and UvrD accessory helicases in *E. coli*, as well as the Pif1 helicase in *Saccharomyces cerevisiae*, perform important roles in helping to clear nucleoprotein complexes (33). More recently, Pif1 has been proposed to be a general displacement helicase for replication bypass of protein blocks, a function similar to the Rep and UvrD helicases (34). These helicases can reduce replisome pausing at several types of native transcription complexes in living cells (13, 22, 35), and of engineered nucleoprotein blocks in biochemical experiments *in vitro* (1, 31).

Rep is the primary accessory helicase in *E. coli*, however, UvrD, a superfamily 1 helicase that translocates 3'-5' along ssDNA, partially compensates for its absence *in vivo,* attributed to the high degree of homology between these two helicases and the abundance of UvrD inside cells (12, 21, 36–38). Rep also promotes replication through stalled transcription elongation complexes (1, 12, 13, 39, 40). UvrD's role in nucleotide excision repair along with UvrABC proteins, as well as in methyl-directed mismatch repair along with the MutHLS proteins, is well characterised (41–46). UvrD interacts directly with RNAP but the functional importance of this interaction has been unclear until recently (47–51) . UvrD has been suggested to promote backtracking of stalled RNAP as a first step in transcription-coupled repair (50, 52); however, other studies argue against UvrD playing any role in coupling nucleotide excision repair to stalled transcription complexes (48, 49, 53–57).

Our aim in this study was to establish the role of UvrD during DNA replication. The primary objective was to test whether UvrD is present at active replication forks using dual-color single-molecule imaging of fluorescently labelled UvrD and replication forks in living *E. coli* cells. We conclude that UvrD is present at replication forks but is not recruited via specific protein interactions with the replisome, which means that it operates in a fundamentally different way to that of Rep. By using super-resolved millisecond single-molecule fluorescence microscopy of mGFP-UvrD in live cells co-expressing a fork marker, DnaQ-mCherry, we show that 80% of DnaQ foci colocalise with UvrD. Stepwise photobleaching intensity analysis reveals tetrameric UvrD foci *in vivo*, to be compared with earlier observations performed *in vitro* using analytical ultracentrifugation that found a mixture of UvrD dimers and tetramers (58). Surface plasmon resonance (SPR) of UvrD in combination with each replisome component identified no specific replisome protein interaction that would explain replisome-UvrD colocalisation. Deletion of Rep, mismatch repair protein MutS and nucleotide excision repair protein UvrA, and disruption of transcription using either mutated RNAP or antibiotic inhibition, significantly reduces the number of UvrD or level of observed colocalisation of UvrD with the fork. Coupled with *in vitro* block-dependent differences in UvrD replication promotion efficiency, we conclude that the colocation of UvrD with the replisome stems primarily from UvrD resolving frequent nucleoprotein blocks to the DNA replication machinery, as opposed to it binding specifically to a replisome component, contrasting distinctly with the replisome-binding mode of operation of Rep.

RESULTS

UvrD is present at the majority of replication forks

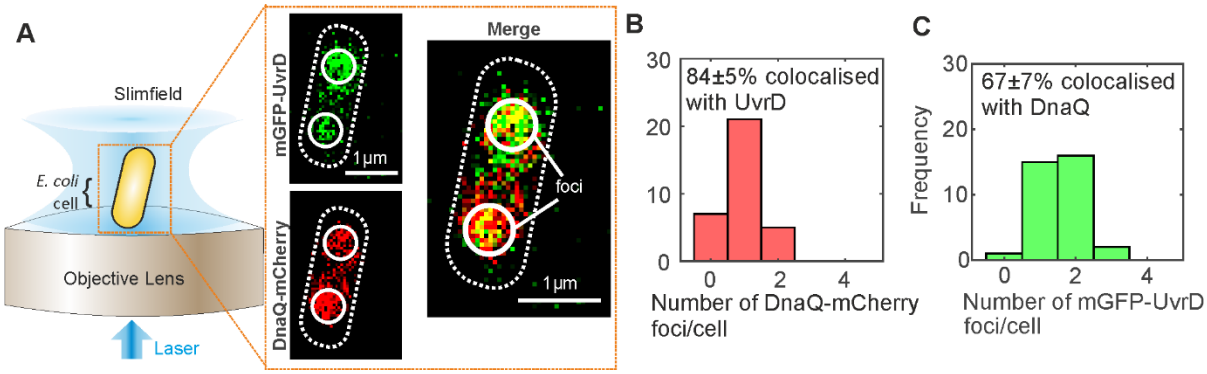

Figure 1: Super-resolved single-molecule light microscopy indicates fork-UvrD colocation. (A). Slimfield microscope schematic and micrographs of mGFP-UvrD, DnaQ-mCherry. Cell membrane and DnaQ/UvrD foci indicated as white dashed and non-dashed lines respectively. (B) and (C) Histogram showing the number of DnaQ and UvrD foci detected per cell respectively, SD errors. N=45 cells.

We investigated UvrD's role in DNA replication using super-resolved single-molecule fluorescence microscopy to track dynamic patterns of fluorescently labelled UvrD localization relative to the replication fork in live cells (Figure 1A). We performed dual-color Slimfield (59, 60) to assess the degree of colocalisation between UvrD and the replisome, using the same imaging protocol used previously to confirm Rep colocalisation with the replisome (13). We employed DnaQ-mCherry as a fork marker - DnaQ encodes a core epsilon subunit of DNAP (13, 61–64) - along with genomically integrated mGFP-UvrD to report on the localization of UvrD. These strains phenocopied wild type for growth and in plasmid loss assays for mGFP-UvrD function retention (Supplementary Figures S1, S2, Tables S1-4). *In vitro* unwinding assays indicate that the nucleoprotein block removal activity of mGFP-UvrD was comparable to wild type (Supplementary Figure S3; note, a summary of all activity comparisons between mGFP-UvrD and wild type UvrD is shown in Table S5). Using Slimfield, we observed 1-2 DnaQ foci per cell, as well as a background 'pool' of unbound DnaQ molecules in the cytoplasm (61), as in the previous study for Rep, corresponding to the two moving forks which appear as a single focus near the start of replication when they are separated by less than the 200-300 nm diffraction limit of our microscope (Figure 1A,B Supplementary Figure S4). We also observed 1-2 UvrD foci per cell (and associated pool), of which 67 ± 7% (±SEM) were colocalised with DnaQ foci and 84 ± 5% of DnaQ foci colocalised with UvrD (Figure 1B and C). We calculated the

133 probability of random overlap between foci by modelling nearest-neighbor separation
134 as a Poisson distribution (65), indicating 20%. To confirm that colocalisation between
135 DnaQ and UvrD was not just a function of the nucleoid association of UvrD, we
136 performed Slimfield on Heat-stable nucleoid-structuring protein (H-NS) tagged with
137 GFP - H-NS associates with the nucleoid but not specifically with the fork - and co-
138 labelled DnaQ-mCherry. We found similar numbers of H-NS foci to UvrD
139 (Supplementary Figure S5) but only 38 ± 4% DnaQ foci were colocalised with H-NS
140 foci implying that, similar to Rep (13), UvrD is present at the majority of forks.
141
142 **UvrD foci are tetrameric assemblies in live bacteria**
143

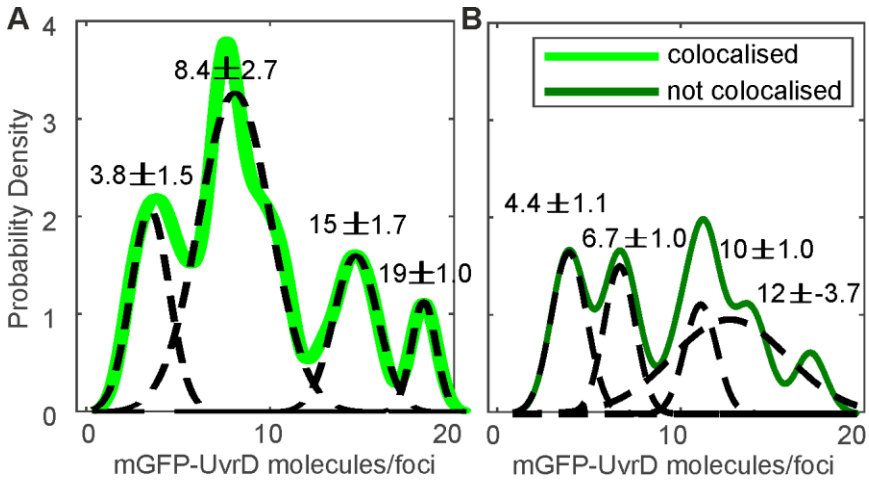

144
145 **Figure 2 UvrD stoichiometry shows tetrameric periodicity.** The distribution of UvrD foci
146 stoichiometry rendered as a kernel density estimate for foci colocalised (A) and not colocalised
147 (B) with DnaQ foci. Distributions were fitted with multiple Gaussian peaks (black dotted lines)
148 with the peak value ± error determined by the half width at half maximum indicated above
149 each peak
150
151 Slimfield also enabled the stoichiometry of these foci (i.e., the number of fluorescently-
152 labelled molecules within each focus) to be determined by utilizing a method involving
153 stepwise photobleaching analysis (61). Here, we determined the brightness of a
154 single-molecule of mGFP or mCherry fluorescent protein using Slimfield
155 (Supplementary Figure S7), and used these values to normalize the initial brightness
156 of tracked foci to estimate the stoichiometry. We found that DnaQ had the same range
157 of 2-6 molecules per focus (Supplementary Figure S8) as found previously,
158 corresponding to 2-3 polymerases per fork (13, 61). The distribution of the
159 stoichiometry of UvrD foci which are colocalised with DnaQ had a distinct lowest-order

160 peak corresponding to approximately four molecules, with subsequent peaks at
161 multiples of four (Figure 2A). UvrD foci that were not colocalised with DnaQ also
162 contained a distinct lowest-order peak at four, but subsequent peaks were less clearly
163 tetrameric.
164 Although we utilised a definitive monomeric variant of GFP which contained an A206K
165 mutation to inhibit dimerization (66), we did not want to dismiss possible non-
166 physiological influences of fluorescent protein labelling of UvrD in its self-assembly
167 process. Using Size Exclusion Chromatography Multi-Angle Laser Light Scattering
168 (SEC-MALLS) we found qualitatively that the majority of UvrD runs off in a monomeric
169 fraction for both purified wild type UvrD and for mGFP-UvrD (Supplementary Figure
170 S9). However, SEC-MALLS has known limitations in differentiating between
171 monomeric and oligomeric fractions due to non-specific binding to the SEC resin
172 (depending on buffering conditions), resulting in proteins eluting later than expected
173 and co-elution of monomeric species and higher mass oligomers. In addition, there
174 are sensitivity difficulties for detecting components present in relatively small
175 quantities – we estimate the error on the cumulative weight fraction to be ~20% on our
176 system, consistent with the reported sensitivity error reported by others (67, 68).
177 To overcome these limitations, we performed high-precision high-sensitivity Slimfield
178 of purified mGFP-UvrD conjugated to a glass coverslip via anti-GFP antibody (69)
179 enabling detection of fluorescent foci bound to the surface with single-molecule
180 sensitivity. Slimfield indicated between ~10-20 surface-bound foci per field of view
181 (Supplementary Figure S9A), whose 200-300 nm width (half width at half maximum,
182 HWHM) was comparable to that determined for single purified GFP molecules. We
183 measured the fluorescence brightness of each focus using the same automated
184 single-particle tracking software as for Slimfield *in vivo* (Supplementary Figure S9B),
185 whose tracks photobleached in a stepwise manner consistent with the presence of
186 just a single GFP molecule. The amplitude of the probability distribution function of
187 foci brightness values (Supplementary Figure S9B) indicated that the proportion of
188 dimers (corresponding to a brightness of approximately twice the modal value) is ~3%
189 that of the corresponding value for monomers. Although it is not possible to entirely
190 exclude non-physiological effects of any fluorescent protein on the cellular activities of
191 a tagged protein, the finding from this single-molecule assay shows that the proportion
192 of monomeric mGFP-UvrD is substantially higher than dimeric mGFP-UvrD and so, if

193 there is an influence of mGFP on the self-assembly process of UvrD, it is unlikely to
194 be a dominant factor.
195 At higher concentrations, UvrD has been observed to exist in a monomer-dimer-
196 tetramer equilibrium *in vitro* (58). DNA unwinding experiments *in vitro* suggest UvrD
197 must function as at least a dimer (70) or a trimer (71), however the oligomeric state of
198 functional UvrD is disputed (reviewed in (72)). Our results are consistent with UvrD
199 existing predominantly as a tetramer, or a dimer of dimers, with multiple tetramers or
200 dimer-dimers sometimes present at forks. It should be noted that we often observe
201 only a single DnaQ focus corresponding to two forks which are separated by less than
202 the diffraction limit of our microscope (Supplementary Figure S8) such that some
203 multiple tetrameric UvrD foci correspond to two replisomes. The less distinct peaks in
204 the UvrD foci that are not colocalised with DnaQ may indicate that other UvrD species
205 (monomers, dimers or trimers) are also present.
206 We determined the total cell copy number of UvrD by estimating the total contribution
207 of mGFP-UvrD fluorescence to the observed intensity in whole cells (73), indicating
208 approximately 800 molecules of UvrD per cell (Supplementary Figure S10), similar to
209 that reported previously for Rep (13), and in line with other proteins that have a small
210 active population detected as foci and a larger population of diffusive molecules in a
211 protein pool (61, 73–76). This is a lower level of UvrD than was reported using
212 transcription rate measurements (77) or high-throughput proteomics (78) but is
213 comparable to recent estimates using ribosome profiling (79).
214
215 **There is no obvious replisome interaction partner for UvrD at the fork**
216 Our earlier findings concerning Rep indicated that colocalisation with the fork and
217 recruitment to the replisome were mediated by protein-specific interaction with the
218 replicative helicase DnaB (80), consistent with Rep and DnaB both exhibiting
219 hexameric stoichiometry (13, 61). We sought to determine whether UvrD is also
220 recruited by interacting with a specific replisome component, expanding on a previous
221 study which used SPR to test whether purified UvrD interacted with each replisome
222 component(12). In this study, UvrD, under conditions consistent with predominantly
223 monomeric UvrD (Supplementary Figure S9), exhibited no direct interaction with
224 primase, SSB, β sliding clamp, the DNA polymerase III αε, χψ or γ complexes; or θ,
225 δ, δ′, χ, and γ subunits (12). However, it did identify a putative weak UvrD-Tau
226 interaction which we interrogated further with more sensitive SPR experiments. We

227 were able to replicate the weak UvrD-Tau interaction; however, as a control we tested
228 Rep and found this also interacted with Tau to a similar extent (Supplementary Figure
229 S11). Tau interactions with either helicase were ~100x lower affinity than UvrD with
230 known interaction partner UvrB (Supplementary Figure S11). We therefore conclude
231 that the Tau interaction with UvrD is likely to be non-specific and that, unlike Rep, UvrD
232 does not have an obvious, direct interaction partner at the replisome, at least from the
233 suite of replisome proteins tested. Since our findings suggest that UvrD may exist as
234 as a tetramer at the replisome, it is also unlikely to be recruited by Rep, which has
235 shown putative interaction (81).
236
237 **The presence of UvrD at the fork is mediated by specific replication blocks**

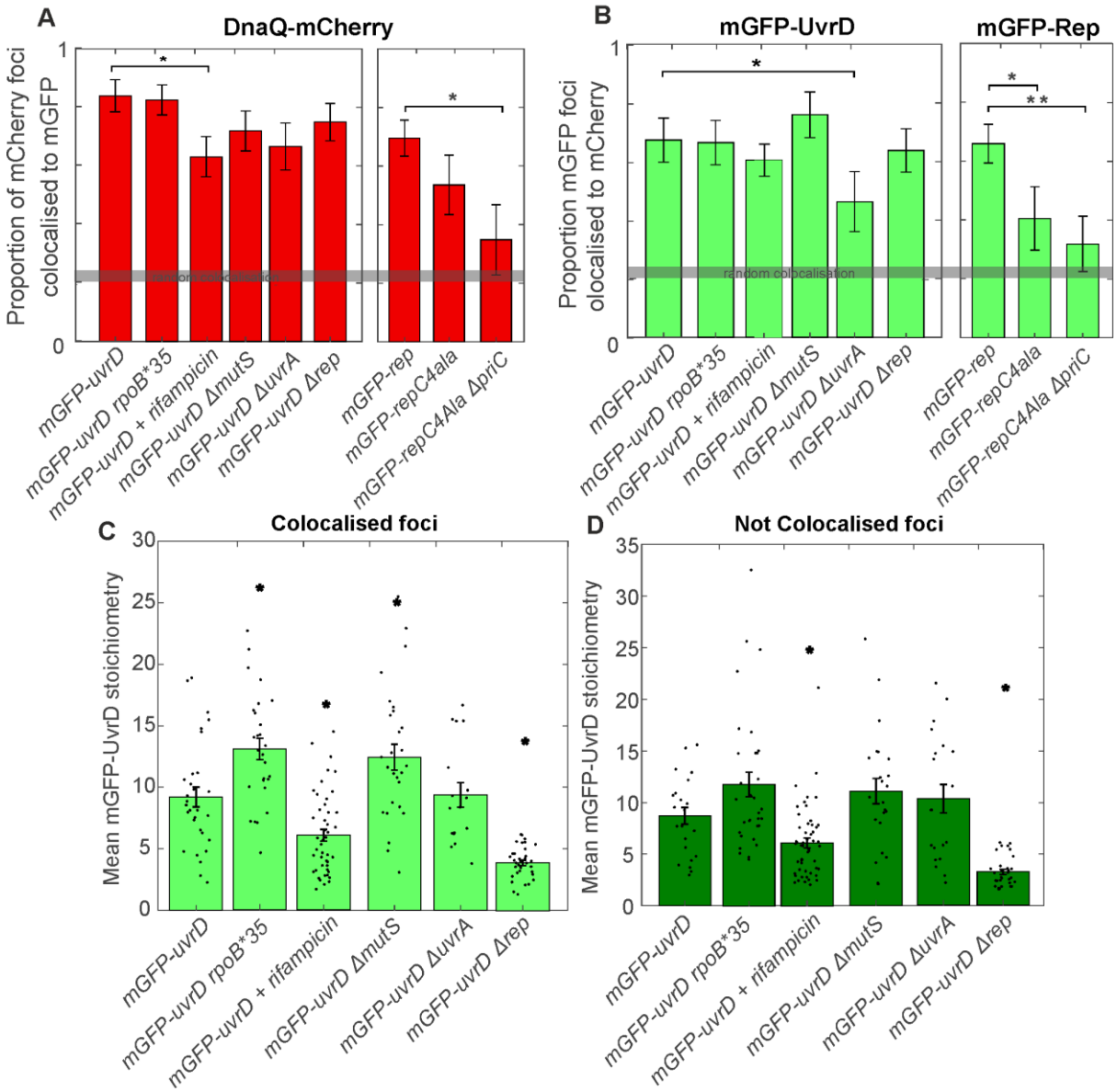

238

239 **Figure 3: Perturbing UvrD function using mutations and rifampicin antibiotic**
240 **intervention influences fork-UvrD colocation**. A. and B. The mean proportion of
241 colocalised DnaQ and UvrD or Rep foci per cell respectively. Error bars represent standard
242 error in the mean and statistical significance by Brunner-Munzel and Student's t-test $p<0.05$
243 indicated by *. Gray bar indicates levels of predicted random colocalisation. C. and D. Jitter
244 plots of colocalised and not colocalised UvrD stoichiometry respectively. Bars show mean
245 UvrD stoichiometry with error bars showing the standard error in the mean and statistical
246 significance by Brunner-Munzel and Student's t-tests $p<0.05$ indicated by *. N=30 cells.
247
248
249 Alternatively, we hypothesized that the association of UvrD with the replication fork
250 might be dependent on its activity in resolving nucleoprotein blocks. To test, we
251 systematically impaired key DNA replication repair processes in which UvrD is
252 implicated, as well as perturbing RNAP replicative blocks by disruption of transcription
253 through both genetic mutation and antibiotic inhibition (Figure 3). We investigated how
254 these perturbations altered fork association through UvrD colocalisation with DnaQ.
255 As a control, we compared these to Rep colocalisation with DnaQ which can be
256 abrogated down to random levels of colocalisation, indicating no interaction with the
257 fork, by mutations which stop Rep interacting with DnaB and PriC (Figure 3A). We
258 perturbed UvrD's activity in resolving DNA damage at replication blocks by deleting
259 *mutS* or *uvrA*, rendering the strains defective in UvrD-associated mismatch repair or
260 nucleotide excision repair respectively (43, 82). We reduced the need for UvrD to
261 remove transcriptional blocks to replication (49) by introducing the *rpoB*35* mutation,
262 which destabilizes open complexes formed during initiation of transcription (83, 84);
263 and by using the antibiotic rifampicin, which blocks elongation of RNA transcripts (85).
264 All of these strains were healthy under normal growth conditions (Supplementary
265 Figure S1, Table S4) and displayed the same phenotype for DnaQ foci number and
266 stoichiometry within measurement error (Supplementary Figure S8).
267 For the transcriptional block perturbations, the *rpoB*35* mutant dual labelled strain
268 exhibited no difference in the proportion of colocalised DnaQ or UvrD foci (Figure 3A
269 and B). This mutant and all others tested exhibited the same predominant tetrameric
270 stoichiometry trends as wild type (Supplementary Figure S12), with clear peaks at
271 tetramer intervals in the colocalised stoichiometry distribution and less clear but still
272 largely tetrameric intervals in the stoichiometry distribution for UvrD foci that are not
273 colocalised with DnaQ. This provides further evidence for tetrameric UvrD assemblies
274 *in vivo*. We compared the mean stoichiometry for each mutant to that of wild type
275 (Figure 3C and D). Unexpectedly, the *rpoB*35* mutant produced a statistically

276 significant increase in mean colocalised stoichiometry, corresponding to
277 approximately one extra UvrD tetramer at the replication fork (Figure 3C). This finding
278 may indicate the level of instability conferred by this mutation has multiple downstream
279 effects that alter UvrD localisation significantly at the fork. Alternatively, it could mean
280 that *rpoB*35* does not affect the formation of the types of transcriptional block that are
281 acted upon by UvrD. Rifampicin treatment produced a clearer response, reducing the
282 number of DnaQ foci colocalised with UvrD by ~20% (Figure 3A) and the mean
283 stoichiometry of colocalised and not colocalised UvrD foci by around one UvrD
284 tetramer (Figure 3C and D). Single-molecule observations of RNAP have shown it to
285 be significantly more mobile under rifampicin treatment (86), implying fewer RNAPs
286 bound to DNA and fewer blocks to replication. Our rifampicin treatment results are
287 consistent with fewer transcriptional blocks to replication reducing the amount of UvrD
288 recruited to the replisome and support the hypothesis that UvrD is recruited by these
289 replicative blocks.
290 By deleting *mutS* or *uvrA* we removed UvrD's role in mismatch repair and nucleotide
291 excision repair respectively. In the Δ*mutS* mutant we observed no change in UvrD
292 colocalisation with DnaQ, but did measure an increase in the mean UvrD stoichiometry
293 colocalised with DnaQ by around one tetramer (Figure 3A). In the Δ*uvrA* mutant we
294 observed a decrease of ~25% in UvrD colocalisation with DnaQ (Figure 3B) with no
295 change in the number of UvrD foci (Supplementary Figure S8). This agrees with a
296 recent model that UvrA and UvrD are continuously associated with a subpopulation of
297 RNAP to form a pre-transcription-coupled-repair complex (pre-TCRC); UvrD is then
298 recruited at DNA lesions to facilitate DNA repair (50).
299 UvrD has been shown to compensate for Rep in *rep* null mutants (12). We also tested
300 what effect this mutation would have in Slimfield *in vivo*. Surprisingly, *rep* deletion
301 resulted in a steep drop in UvrD copy number (Supplementary Figure S10). The
302 degree of colocalisation between UvrD and DnaQ remained unchanged compared to
303 wild type (Figure 3A and B) but foci stoichiometry was reduced to a single UvrD
304 tetramer (Figure 3C and D and Supplementary Figure 11), consistent with the
305 observed lower copy number and availability of UvrD. The drop in UvrD copy number
306 may reflect complex regulatory shifts in response to losing a key protein in Rep,
307 although it is interesting that even at low copy numbers, a UvrD tetramer remains

308 recruited to the fork. Double knockouts, deficient in both Rep and UvrD, are lethal (12)
309 so this minimal helicase presence must be the limit required for survival.
310

311 **Dynamic association of UvrD with the fork depends on DNA repair processing**

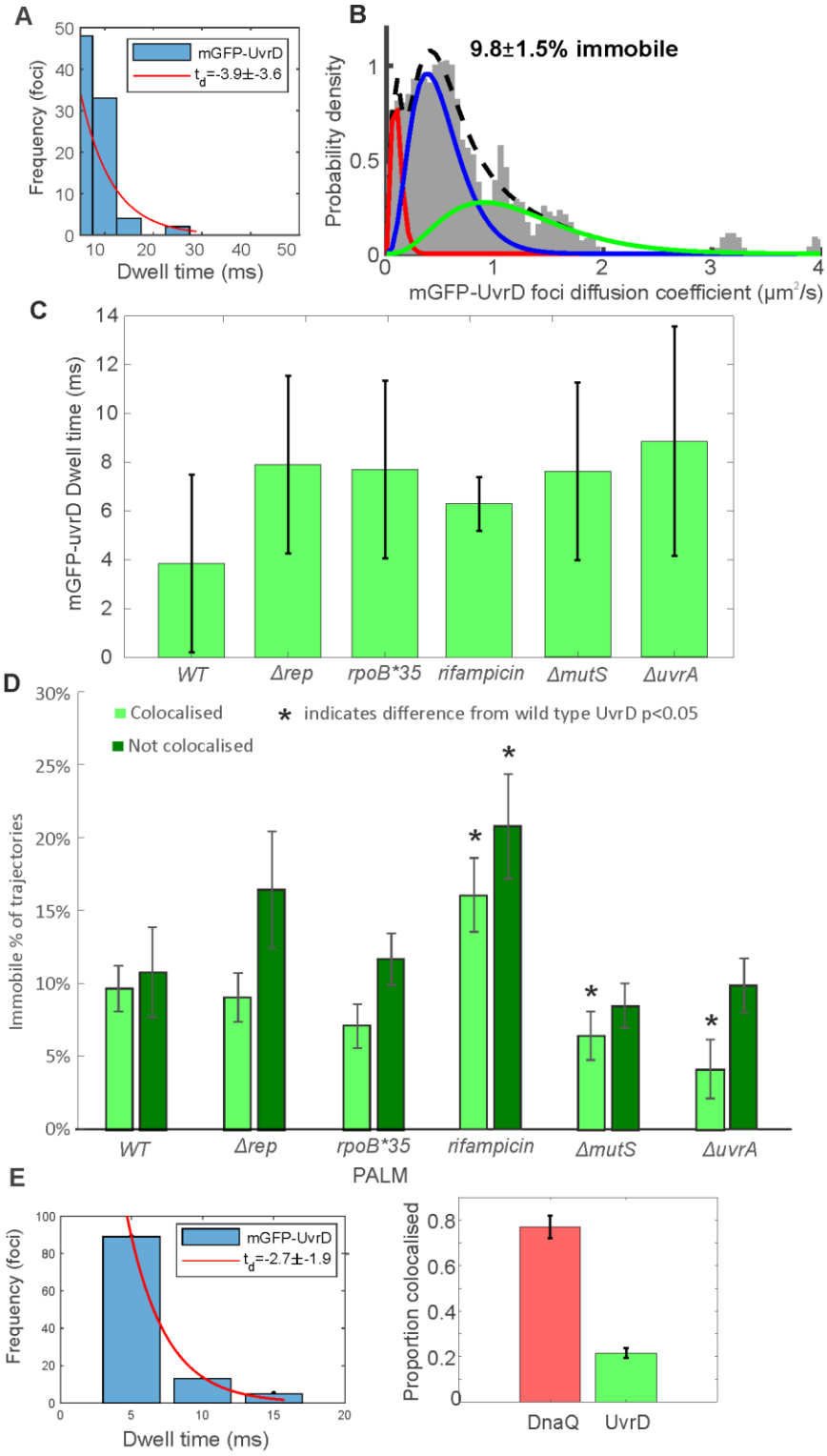

312

313 **Figure 4: UvrD dynamics are heterogeneous.** A. Distribution of time over which UvrD and
314 DnaQ foci were colocalised (blue) fitted with an exponential (red) to yield a characteristic
315 dwell time. B. Distribution of microscopic diffusion coefficients of wild type UvrD foci (gray)
316 fitted with a three-state gamma distribution model containing a relatively immobile population
317 with D = 0.1 μm²/s (red), a transiently immobile population, D = 0.5 μm²/s (blue) and a mobile
318 population, D=1.2 μm²/s (green). C. The dwell times for each UvrD strain. Error bars represent
319 the 95% confidence intervals on the fit. D. The proportion of UvrD foci in the immobile

population for each UvrD strain colocalised or not colocalised with DnaQ foci location. Statistically significant differences $p<0.05$ from wild type indicated by *. E. PALM dwell time and colocalisation proportion of detected tracks. N=45 cells for wild type and 30 per mutant, with ~300 trajectories.

By tracking UvrD foci, we were also able to characterize their dynamics in wild type and repair impaired cells. We measured the exposure time per frame multiplied by the number of image frames in which UvrD foci were colocalised with DnaQ foci and fitted the distribution of these dwell times with a single exponential function. We also calculated the apparent microscopic diffusion coefficient of individual foci (Figure 4 and Supplementary Figure S13). The mean UvrD dwell time at the fork (corresponding to the exponential fit time constant) for the wild type strain was measured to be approximately 4 ms, indicating a relatively dynamic association of UvrD at the replication fork. The diffusion coefficients (*D*) were best fit with a three parameter Gamma model, containing immobile (D = 0.1 $\mu m^2/s$), transiently immobile population (D = 0.5 $\mu m^2/s$) and mobile (D = 1.2 $\mu m^2/s$) populations similar to Rep. In wild type, we found that approximately 10% of UvrD foci were immobile, whether colocalised with the fork or not, with the remaining foci split between the other two populations.

We applied the same approach to cells which had been perturbed using either a range of mutations which were known to affect DNA replication repair and block resolution, or antibiotic treatment known to affect expression of RNAP. All perturbations resulted in a marginal though statistically insignificant increase in mean dwell times to between 6-9 ms. The Δ*rep* and *rpoB*35* mutations resulted in no change in mobility from wild type. Rifampicin treatment however, resulted in an increase in the proportion of immobile foci both at and away from the fork. This finding appeared at first counterintuitive since rifampicin treatment results in more mobile RNAP (86), however it is unclear what effect rifampicin has on the population of RNAP molecules that remain bound to DNA. These results may suggest that such blocks provide an increased barrier to replication, decreasing UvrD mobility as it attempts to resolve blocks. In Δ*mutS* and Δ*uvrA* strains, the proportion of immobile foci decreased at the fork, again consistent with the hypothesis that UvrD association with the fork is dependent on DNA damage resolution activity. One alternative explanation for these results is that UvrD is less mobile when resolving DNA damage blocks to replication and more mobile when resolving transcriptional blocks, as reducing or eliminating

354 UvrD's role in these processes decreased or increased the immobile fraction in DNA
355 repair and transcription impaired cells respectively (Figure 4).
356
357 ***In vitro* biochemical experiments support the block-dependent UvrD function**
358 **model**
359 To investigate the role of different nucleoprotein blocks in UvrD recruitment to the
360 replisome, we reconstituted replisomes on plasmid templates containing *oriC* and
361 block sites. This *in vitro* approach allowed us to specify the type of nucleoprotein block
362 and test whether the ability of UvrD to promote replication is affected by whether UvrD
363 recruitment occurs before or after the replisome encounters the block. In these
364 experiments, UvrD or a Rep control were included either from the start of replication,
365 or were added after the replisome encountered the nucleoprotein block. Blocked fork
366 resolution was probed by examining replication products using denaturing gel
367 electrophoresis.
368 We first generated stalled transcription elongation complexes using the $P_{lacUV5\ 52C}$
369 promotor which allows RNAP to be stalled via nucleotide deprivation. The $P_{lacUV5\ 52C}$
370 promotor contains no C residues between +1 and +52 on the non-transcribed strand,
371 enabling transcription to be stalled by the omission of CTP. Stalled RNAP acts as a
372 barrier to the replisome in both head-on and co-directional orientations and prevents
373 the formation of full-length replication products (1). Arresting the replisome at this
374 RNAP block resulted in replication products consisting of four truncated leading
375 strands. The strand sizes matched those expected for replisomes moving clockwise
376 or counter-clockwise from *oriC* and encountering $P_{lacUV5\ 52C}$ or the promoters within the
377 *ColE1* plasmid origin of replication (Figure 5A, lane 2 and Figure 5C) (1). As previously
378 found, inclusion of Rep or UvrD promotes movement of replisomes through stalled
379 RNAP (1). This is shown by a decrease in all four truncated leading strand products
380 and a concomitant increase in production of full-length leading strands (Figure 5A,
381 lanes 3 and 5 and 5E) (1). Addition of UvrD once the replisome had already
382 encountered the block gave variable results that ranged from an inhibitory to a stronger
383 effect, although differences were not statistically significant at $p<0.05$ (Figure 5A,
384 compare lane 5 with 6, Figure 5E). Similar results were also obtained for Rep (Figure
385 5A, compare lane 3 with 4, Figure 5E). Neither Rep nor UvrD are capable of pushing
386 stalled RNAP from the $P_{lacUV5\ 52C}$ stall site in the absence of replication, so these
387 results are dependent on active replisomes encountering blocks (1).

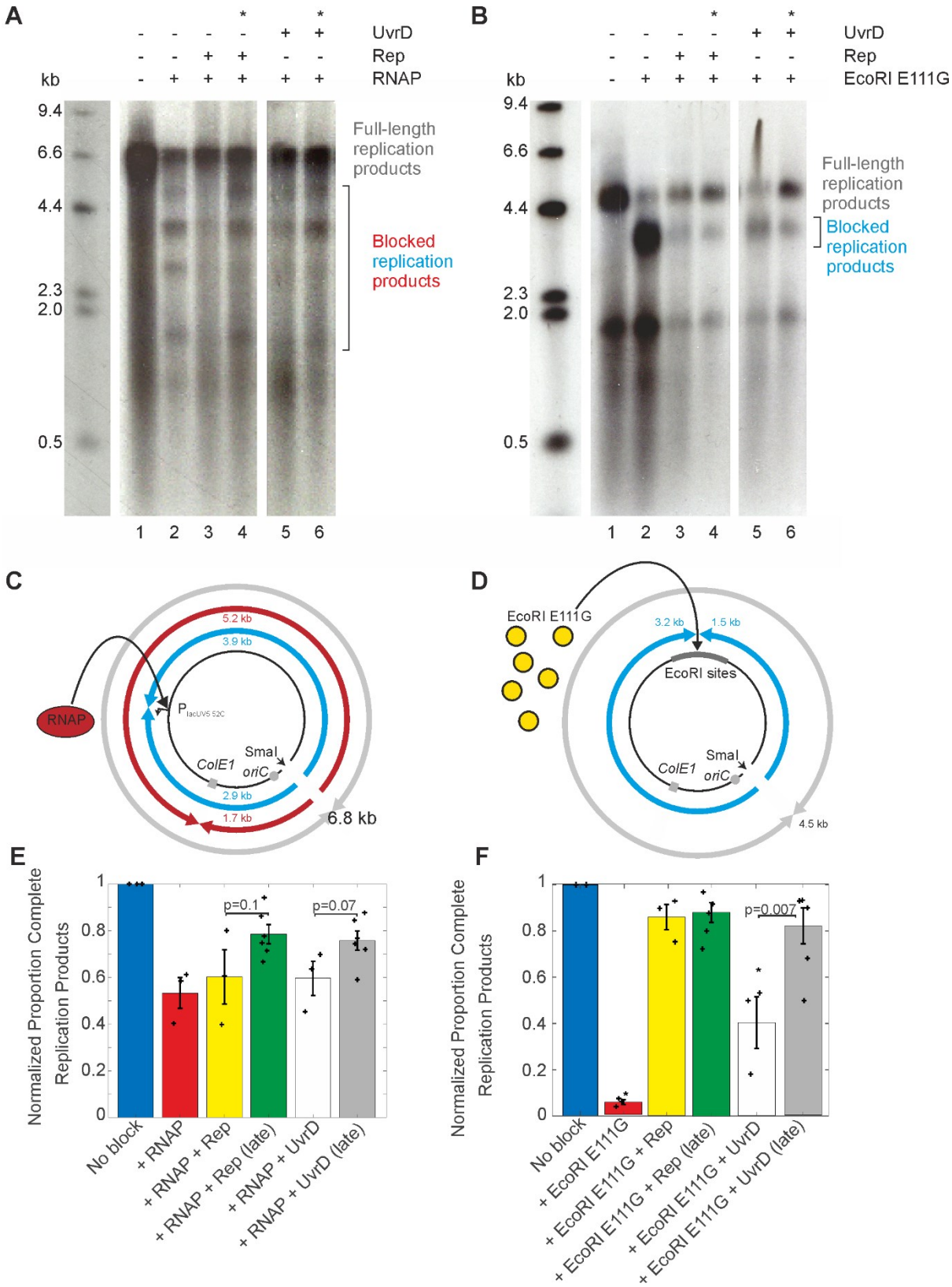

Figure 5: Helicase pre-association affects the promotion of replication fork movement through different nucleoprotein blocks A. Denaturing agarose gel of replication products formed from pPM872 (1) in the absence and presence of RNAP block, Rep and UvrD added pre- and post-collision (*) as indicated. B. Denaturing agarose gel of replication products formed from pPM594 (12) in the absence and presence of EcoRI E111G block, Rep and UvrD added pre- and post-collision (*) as indicated. Truncated leading strand products formed by

395 replisomes originating from *oriC* and colliding with RNAP (C) and EcoRI E111G (D).
396 Quantification of lanes in (A) and (B) from three technical replicates shown in (E) and (F),
397 with standard error in the mean indicated and each replicate result shown as a cross. Note, we
398 were also able to confirm that the mGFP tag used in the UvrD microscopy experiments does
399 not prevent UvrD from dislodging nucleoprotein blocks in this context (see Supplementary
400 Figure S14).
401

402 Since UvrD has been shown to interact with RNAP (47–49), we reasoned that it could
403 be quickly recruited to an RNAP block no matter the time of addition. We used a
404 different nucleoprotein block that does not bind UvrD to test whether UvrD-block pre-
405 association is a requirement for its promotion of replication. Modified restriction
406 enzymes are a useful model for nucleoprotein blocks because their block strength can
407 be modified by varying the number of recognition sites on DNA templates. We chose
408 a mutant restriction enzyme (EcoRI E111G) that binds to its recognition sequence but
409 has reduced cleavage activity (87). EcoRI E111G blocks to replication can be removed
410 by Rep or UvrD helicase activity (12). We tested whether UvrD or a Rep control could
411 promote replication through an array of eight EcoRI sites when added before or after
412 initiation of replication (Figure 5B and D). Rep promotion of replication through this
413 barrier was unaffected by time of addition (Figure 5B, lane 3 and 4, 5F). Presumably
414 this is because the Rep-DnaB interaction ensures it will always be present at
415 replication fork blocks as it travels with the replisome. Surprisingly, adding UvrD post-
416 collision did not impede its promotion of replication; in fact, the resolution of these
417 collisions appeared to be more efficient because the proportion of full-length
418 replication products increased (Figure 5B, compare lane 5 with 6, 5F). Quantification
419 of full-length replication products as a proportion of reaction products showed that late
420 UvrD addition increased full-length replication products to 84% (n=6) compared to
421 41% (n=3) when UvrD was present before fork collision. This contrasts with the RNAP
422 block results where the UvrD-RNAP interaction (47–50) might be responsible for
423 localising UvrD to the block and facilitating resolution, resulting in no difference when
424 present pre- or post-collision. Similarly, Rep associates directly with the replication
425 fork, resulting in no difference when present pre- or post-collision, for both blocks.
426 These results support the absence of a UvrD-replisome interaction and suggest that
427 UvrD might be recruited to stalled replication forks at nucleoprotein blocks using a
428 different mechanism than Rep. We have no direct evidence to support a hypothesis
429 that UvrD recognises a specific DNA structure at a blocked fork, and note previous
430 studies which indicate no binding specificity to DNA beyond requiring 3′ssDNA (88,

431 89). Combining these data with reductions in colocalisation between UvrD and DnaQ
432 fork marker when replication blocks are perturbed *in vivo*, leads us to propose that
433 UvrD is present at the replication fork due to the high frequency of different types of
434 blocks to replication.
435
436 **DISCUSSION**
437 Here, we show that most replisomes are associated with UvrD. However, unlike the
438 established Rep association, UvrD has no replisome interaction partner. UvrD instead
439 associates with the replisome through the frequent blocks to replication encountered
440 by the fork. Similarly to Rep, *in vitro* evidence suggests that UvrD functions poorly as
441 a helicase when it is monomeric (90). We showed previously that functional Rep foci
442 are hexameric *in vivo* but that this oligomerisation state is due to interactions with the
443 hexameric DnaB replicative helicase (13). Again, UvrD functions differently and
444 appears to self-associate into tetramers, as evidenced in our findings by tetrameric
445 periodicity both at and away from the fork (Figure 2 and Supplementary Figure 11),
446 consistent with previous ultracentrifugation experiments *in vitro* (58). It is possible that
447 UvrD may not have evolved to fulfil exactly the same functions as Rep; in many
448 enzyme-catalysed reactions, if one enzyme is depleted then another will be available
449 to take its place, but with a reduced catalytic efficiency (91). On initial inspection, this
450 might appear to be the case for Rep and UvrD, in light of the lower efficiency of block
451 resolution for UvrD compared to Rep, noting that Rep deletion has a profound impact
452 on replication whereas UvrD deletion does not (92). However, we find that Rep and
453 UvrD do have different modes of colocation at a replication block. These differing
454 mechanisms of replication promotion suggest a model in which different accessory
455 helicases have evolved to fulfil the same overall function of resolving a block to DNA
456 replication but in alternative ways. Even with different block removal efficiency, such
457 redundancy may confer increased robustness, helping to ensure that DNA replication
458 is carried out correctly.
459 We used single-molecule Slimfield to show that a high proportion of forks are
460 colocated with UvrD *in vivo.* Although the raw imaging data is still subject to diffraction-
461 limited resolution, localization tracking algorithms pinpoint fluorescently labelled UvrD
462 to 40 nm lateral precision, smaller than the 50 nm diameter of the replisome machinery
463 itself (61) and equivalent to ~100 bp DNA. Thus, our measurements for UvrD and
464 DnaQ are good indicators of genuine colocation of UvrD and the fork. Importantly, the

465 degree of colocation we observed is much higher than expectations of random overlap
466 of the optical images of DnaQ-mCherry and mGFP-UvrD.

467 Using SPR analysis we failed to find evidence for direct interaction partners at the
468 replisome apart from the Tau protein. However, as a control, we tested Tau's
469 interaction with Rep and also found a positive interaction. Thus, we conclude that the
470 interaction of UvrD with Tau is most likely non-specific and that UvrD recruitment to
471 the replisome is mediated by blocks, rather than by a specific replisome interaction
472 partner. A practical limitation of SPR measurement is that the immobilisation
473 procedure does not normally preserve oligomer subunit interactions if they are not
474 very tight, so one would expect to observe UvrD monomers on the surface. Where
475 detection of an oligomer is specifically required, optimisation must be performed to
476 stabilise it (e.g. cross-linking) for immobilisation. It is possible at very high
477 immobilisation levels to have some "apparent" oligomer generated simply by the
478 proximity of subunits but this is not a practically useful strategy. UvrD's tetrameric form
479 may also affect its interactions with replisome components. These limitations mean
480 that SPR alone is semi-quantitative in not having the capability to report on the precise
481 oligomeric state of UvrD on the SPR chip.

482 We probed UvrD's function at the replication fork by perturbing its known DNA repair
483 processing functions, knocking out *mutS* and *uvrA* to block mismatch and nucleotide
484 excision repair respectively. We also introduced a mutant RNAP with *rpoB*35* and
485 treated the wild type with rifampicin to reduce the occurrence of transcriptional blocks
486 to translocating replication machinery. Deleting *uvrA* and rifampicin treatment
487 produced clear results, reduced fork colocalisation, but deleting *mutS* and introducing
488 the *rpoB*35* mutation did not. However, these latter perturbations did result in an
489 identical phenotype of one extra UvrD tetramer per fork. Indeed, a recent study has
490 confirmed the continuous physical association of UvrA and UvrD with RNAP. Our
491 results are in agreement with their model proposed that UvrA and UvrD form a pre-
492 TCRC that subsequently facilitates recruitment of UvrD at sites of DNA lesions.(50)
493 The *rpoB*35* mutation improves cell viability to increased DNA lesions (83). Taken
494 together, our results indicate that transcription-mediated lesions are a frequent
495 impediment to active replisomes resulting in transcription-replication conflicts, that
496 UvrD helps to clear via its association with RNAP. This intriguing link between

497 mutations requires further study, possibly of these dual labelled strains in response to
498 increased DNA lesions.
499 The only function of UvrD we did not probe directly was its role in RecA-mediated
500 recruitment. We believe the results from a *recA* knockdown would be difficult to
501 interpret due to its pleiotropic effects. RecA is the principal recombinase and induces
502 the complex SOS response resulting in the induction of UvrD expression (93, 94).
503 Furthermore, UvrD removes RecA from RecA-DNA complexes, thus functioning as an
504 antirecombinase (95–97). Dissecting these UvrD functions from other effects that a
505 *recA* mutation may have on the cell would be difficult. Applying the perturbations in
506 combination, i.e. double knockdowns or knockdowns plus rifampicin, would likely lead
507 to confusing results since too many deleterious perturbations may be lethal or change
508 normal cell function too radically to be biologically relevant in the intended way.
509 For the suite of mutant strains investigated we found small but significant
510 colocalisation changes in UvrD, implying that UvrD-fork colocation is due to the
511 frequent blocks to replication it encounters. Recent biochemical findings *in vitro* show
512 that blocks to replication occur very frequently (1, 19, 98) potentially accounting for our
513 observations here.
514 We show that forks stalled at transcriptional blocks can be rescued by addition of
515 UvrD, prior to or post-stalling. If UvrD is to help perform this function then it must be
516 present during the resolution of collision between the replication and transcription
517 machinery, however, our estimate for dwell time at the fork of just a few milliseconds
518 - compared to seconds for DnaQ (62) - suggests a non-negligible dissociation
519 constant; UvrD is not processive *per se* but undergoes rapid turnover at the fork such
520 that there is a high likelihood for UvrD being present at any given time, but not
521 necessarily the same set of molecules. Interestingly, we observed a similar dwell time
522 for Rep (13), despite it having a clear association partner in DnaB at the fork. However,
523 using a defective restriction enzyme EcoRI E111G block produced a different effect,
524 with late UvrD addition improving block resolution. This restriction enzyme block is
525 artificial and less biologically relevant but may indicate that the known specific UvrD
526 interaction with RNAP is important. Improved replication resolution with late addition
527 of UvrD is intriguing, implying increased affinity for, or activity at, pre-stalled replication
528 forks compared to UvrD being present as the fork stalls. Complete understanding
529 requires further study of replication block resolution in different conditions.

530 Our findings suggest that UvrD diffuses and transiently interacts with DNA either at
531 random, through interactions with RNAP, or interactions with a specific conformation
532 of the blocked replication fork. At the DNA, UvrD is predominantly tetrameric, either
533 pre-assembling in solution or on the DNA itself. The frequent sampling leads to UvrD
534 often being in the vicinity of the replisome, allowing UvrD to resolve frequent blocks to
535 replication. It is also possible that certain barriers to replication may be harder for Rep
536 to resolve, and such barriers can be more efficiently removed by UvrD, however, it is
537 still likely that they do not change the cell's ability to replicate the genome in light of
538 *uvrD* deletion still resulting in viable cells. Indeed, UvrD shares a high degree of
539 structural similarity with Rep, although the two proteins differ significantly in their amino
540 acid sequences (31, 99). While Rep is recruited to the fork through specific interactions
541 with DnaB, no such interactions were found for UvrD. Stochastic impairment of the
542 ability of Rep to interact with DnaB may necessitate block processing at the fork by
543 UvrD. In summary, our results highlight the contribution of UvrD action to facilitating
544 accurate genome duplication at active replisomes.

545 **Acknowledgments**

546 We thank Maria Chechik for help with mGFP-UvrD purification. We thank Prof. Nigel
547 Savery (University of Bristol) for the gift of the pETDuet-UvrD overexpression plasmid,
548 and Dr Chris Hill (University of York) for the donation of ^{32}P. We thank the Molecular
549 Interactions Laboratory in the Bioscience Technology Facility at the University of York
550 for technical assistance and support. Supported by BBSRC via grants BB/N006453/1
551 (M.L., P.M.), BB/R001235/1 (M.L.,P.M.), BB/N014863/1 (M.H.).

552

553 **Author Contributions**

554 Conceptualization: AJMW, AS, PMG, MH, MCL
555 Methodology: AJMW, AS, JALH, AL, CG, PMG, MH, MCL
556 Software: AJMW
557 Investigation: AJMW, AS, JALH, APD, AL, DW, CG, MH
558 Visualization: AJMW, AS, MH
559 Supervision: AJMW, AS, MH, PMG, MCL
560 Writing—original draft: AJMW, AS, MH, MCL

561 Writing—review & editing: AJMW, AS, JALH, AL, DW, PMG, MH, MCL
562
563 **Declaration of interests**
564 The authors declare no competing interests.
565

566 **MATERIALS AND METHODS**

567 **Strain construction**

568 All strains used in this study (listed in full in SI Table S1, with associated plasmids
569 and primers in SI Tables S2 and S3) are derivatives of the laboratory wild type strain
570 TB28. Tagging of *dnaQ-mCherry-<kan>* (C-terminally labelled) is described in (13).
571 *mGFP-uvrD-<kan>* (N-terminally labelled) was amplified from plasmid pAS79 (*uvrD*$^{+}$)
572 with primers oAS145 and oJGB383 having 50 bp homology to either end of the
573 native *uvrD* locus. The resulting PCR product had homology either side such that
574 recombination with the chromosome would result in integration of the PCR product at
575 the native locus under the control of the native promoter. Prior to integration, all PCR
576 products were treated with DpnI, gel purified, and introduced by electroporation into
577 cells expressing the lambda Red genes from the plasmid pKD46 (55). The
578 recombinants were selected for kanamycin resistance and screened for ampicillin
579 sensitivity. The colonies obtained were verified for integration by PCR and
580 sequencing. The *uvrD* recombinants were verified by PCR amplification using
581 primers oPM319 and oPM320, and sequencing using the primers oJGB417,
582 oJGB418, oPM407, oPM409, oPM411, and oMKG71. Where required, the
583 kanamycin resistance gene was removed by expressing Flp recombinase from the
584 plasmid pCP20 (100) to generate kanamycin sensitive strains carrying the
585 fluorescent protein (FP) fusions. Dual labelled strains were created by introducing
586 the kanamycin tagged FP alleles by standard P1 mediated transduction into single
587 labelled strains carrying the required FP allele after removing the linked kanamycin
588 marker.

589 **Determination of cell doubling time**

590 *E. coli* strains were grown overnight in LB medium at 37°C at 200 rpm shaking. The
591 saturated overnight cultures were diluted 100-fold into fresh LB or washed once with

592 1X 56 salts and diluted 100-fold in fresh 1X 56 salts with 0.2% glucose as the carbon
593 source. Aliquots of 100 µl each of the diluted cultures in fresh media were pipetted
594 into individual wells of 96 well clear flat bottom sterile microplates (Corning). The
595 microplates containing the diluted cultures were incubated in a BMG LABTECH
596 SPECTROstar Nano microplate reader at 37°C and the optical density (OD_{600})
597 values were recorded at defined time intervals. The time taken for the optical density
598 values to increase 2-fold during the exponential growth phase of the culture was
599 taken as the cell doubling time (SI Table S4, Supplementary Figure S1).

600 **Protein Overexpression and Purification**

601 *mGFP-uvrD* was excised from pAS79 using XhoI and SalI and ligated into pET14b
602 cut with XhoI, creating pAS152 encoding N-terminal histidine-tagged mGFP-UvrD.
603 pAS152 was used to overexpress the His-mGFP-UvrD fusion in BL21(DE3)/pLysS.
604 A single colony was used to inoculate 10 mL of LB containing carbenicillin and
605 chloramphenicol at 50 µg/mL and was incubated overnight at 37°C and 180 rpm.
606 The overnight culture was clarified by centrifugation at 3,220 xg and 4°C, before the
607 pellet was resuspended in 1 mL of LB and used to inoculate 1 L of LB containing
608 carbenicillin and chloramphenicol at 50 µg/mL. The culture was then incubated at
609 37°C and 180 rpm until an OD_{600} of 0.6, at which point it was cooled to 20°C and
610 IPTG was added to a 1 mM final concentration and incubation was continued at
611 20°C and 180 rpm overnight. Cells were pelleted by centrifugation at 3,500 xg and
612 4°C for 20 minutes, the pellet was resuspended in 20 mL of 50 mm Tris-HCl, pH 7.5,
613 at 4 °C, and 10% sucrose (w/v) before flash freezing with liquid nitrogen and storing
614 at -80°C.

615 Cells were thawed on ice and Tris pH 8.3, EGTA, EDTA, DTT, NaCl and lysozyme
616 were added to final concentrations of 50 mM, 0.5 mM, 5 mM, 1 mM, 200 mM and 0.2
617 mg/mL respectively. The suspension was incubated on ice for 30 minutes before the
618 addition of sodium deoxycholate to a final concentration of 0.05% (w/v) and allowed
619 to stand on ice for a further 30 minutes. NaCl was then added to a final concentration
620 of 500 mM before lysis by sonication on ice. The sample was clarified by
621 centrifugation at 30,600 xg and 4°C for 20 minutes and the supernatant collected.
622 The supernatant was subjected to polymin P precipitation, polymin P was added
623 dropwise to a final concentration of 0.075% (w/v) under stirring at 4°C, stirring was

624 continued for 10 minutes before centrifugation at 30,600g and 4°C for 20 minutes.
625 The supernatant was collected and ammonium sulfate was added gradually to it
626 whilst stirring at 4°C to a 50% saturation, the pellet was collected by centrifugation
627 as previously and resuspended in binding buffer (20 mM Tris pH 8.3, 500 mM NaCl)
628 + 5 mM imidazole. The sample was loaded onto a 5 mL HisTrap FF column that had
629 been pre-equilibrated with binding buffer + 5 mM imidazole. The column was then
630 washed with 15 column volumes of binding buffer + 5 mM imidazole before it was
631 developed with a 20-column volume gradient of binding buffer + 5 to 300 mM
632 imidazole. Peak fractions were monitored by their green colour as well as by SDS-
633 PAGE, the peak fractions containing his-mGFP-UvrD were pooled and diluted in
634 buffer A (20 mM Tris pH8.3, 1mM EDTA, 0.5 mM EGTA, 1mM DTT) to a conductivity
635 equivalent to that of buffer A + 100 mM NaCl. The peak fractions were then loaded
636 onto a 5 mL HiTrap Q column equilibrated with buffer A + 100 mM NaCl, the column
637 was washed with 10 column volumes of buffer A + 100 mM NaCl and a gradient from
638 10 mM to 650 mM NaCl was developed over 20 column volumes. Peak fractions
639 were assessed by SDS-PAGE and those containing his-mGFP-UvrD were loaded
640 onto a HiLoad 26/60 Superdex 200 gel filtration column equilibrated with buffer B (20
641 mM Tris pH8.3, 300 mM NaCl), the column was developed with buffer B and peak
642 fractions containing pure his-mGFP-UvrD as determined by SDS-PAGE were pooled
643 and loaded onto a 5 mL HisTrap FF column that had been pre-equilibrated with
644 binding buffer + 5 mM imidazole. The column was then washed with 3-column
645 volumes of binding buffer + 5 mM imidazole before it was developed with a 6-column
646 volume step of binding buffer + 200 mM imidazole. Peak fractions were then
647 dialysed against storage buffer (20 mM Tris pH8.4, 300 mM NaCl, 10% glycerol)
648 aliquoted and flash frozen in liquid nitrogen before storing at -80°C. Protein
649 concentration was determined by Bradford's assay.

650 UvrD was purified as previously described (56). Briefly UvrD was overexpressed in
651 BL21-AI from a pETDuet vector, via induction by IPTG and arabinose. UvrD was
652 purified from the soluble cell extract after lysis through the use of affinity (heparin
653 agarose), anion exchange (Q-sepharose), and gel filtration chromatography. Pure
654 UvrD was then stored at -80ºC after dialysis into storage buffer or used immediately
655 in Size Exclusion Chromatography - Multi-Angle Laser Light Scattering (SEC-

656 MALLS) analysis or subsequently diluted to 1 nM for single-molecule *in vitro*
657 experimentation.

658 Biotinylated UvrD and Rep were purified as previously described (12). Briefly, the
659 proteins were overexpressed in a BL21 (DE3) containing pBirAcm, encoding a biotin
660 ligase via induction by IPTG and the addition of biotin to the growth media. The
661 biotinylated proteins were then purified from the soluble cell extracts by ammonium
662 sulphate precipitation, and affinity chromatography (softlink avidin and heparin
663 agarose). Pure proteins were then dialysed into storage buffer overnight and stored
664 at -80°C

665 **Helicase assay**

666 Assays for unwinding of streptavidin-bound forks were performed using a substrate
667 made by annealing oligonucleotides oPM187B20 (5' end labelled with ^{32}P) and
668 oPM188B34. Reactions were performed in 10 µL volumes containing 40 mM HEPES
669 (pH 8); 10 mM DTT; 10 mM magnesium acetate; 2 mM ATP; 0.1 mg ml^{-1} BSA and
670 1 nM forked DNA substrate. Reactions were carried out as described earlier (13,
671 101). Briefly, the reaction mixture was pre-incubated at 37°C for five minutes with or
672 without 1 µM streptavidin (Sigma-Aldrich), to which helicase (as indicated) and biotin
673 (Sigma-Aldrich) were added to 100 µM (acting as a trap for free streptavidin) and
674 incubated at 37°C for another 10 minutes. Reactions were stopped by addition of 2.5
675 µl of 2.5% SDS, 200 mM EDTA and 10 mg ml^{-1} of proteinase K. Reactions were then
676 analysed by non-denaturing gel electrophoresis on 10% polyacrylamide TBE gels.
677 The quantification of the unwinding and displacement of streptavidin from the fork
678 was carried out as described in (102).

679 **Preparation of cells for microscopy**

680 Cells were grown overnight in LB to saturation. The overnight cultures were
681 inoculated the next day at 1:1000 dilution in 1X 56 salts supplemented with 0.2%
682 glucose as the carbon source. The dilutions were then grown at 30°C to mid-log
683 phase.

684 **Rifampicin treatment**

685 Cells prepared for microscopy were treated with rifampicin at a final concentration of
686 50 µg/mL for 30 minutes at 30°C.

687 **Microscopy and image analysis**

688 Imaging was performed on a bespoke dual-colour single-molecule microscope (13).
689 Excitation from Obis 488 nm and 561 nm wavelength 50mW lasers (run at 20 mW)
690 was reduced to 10 µm at full width half maximum field in the sample plane producing
691 Slimfield (59) producing a mean excitation intensity of ~0.25 mW/µm^2. Lasers were
692 digitally modulated to 5 ms period to produce alternating laser excitation using
693 National Instruments dynamic I/O module NI 9402. Excitation was coupled into a
694 Zeiss microscope body with the sample mounted on a Mad City Labs nanostage.
695 Images were magnified to 80nm/pixel and imaged using an Andor Ixon 128 emCCD
696 camera. Color channels were split red/green using a bespoke color splitter consisting
697 of a dual-pass green/red dichroic mirror centered at long-pass wavelength 560 nm
698 and emission filters with 25 nm bandwidths centered at 542 nm and 594 nm.

699 Cells were imaged on agarose pads suffused with minimal media as described
700 previously (103). Foci were detected and tracked using previously described
701 bespoke MATLAB software (104). In brief, bright candidate foci were detected in
702 each frame by image transformation and thresholding based on Otsu's method. A
703 17x17 pixel region of interest (ROI) is drawn around each candidate to define the
704 local background, while a radius 5 circle is drawn in the center (the foreground) and
705 subjected to iterative Gaussian masking (69). Foci were accepted if their signal to
706 noise ratio was above 0.4, defined as the mean intensity inside the foreground
707 divided by the standard deviation of the local background. Foci in successive frames
708 were linked together into trajectories based on nearest distance, provided it was < 5
709 pixels. Linked foci were accepted as "tracks" nominally if they persist for at least 4
710 consecutive image frames.

711 Characteristic intensity of mGFP or mCherry was determined from the distribution of
712 foci intensity values towards the end of the photobleach confirmed by overtracking
713 foci beyond their bleaching and applying an edge-preserving filter (105, 106) to the
714 raw intensity data to generate individual steps of the characteristic intensity, due to
715 photobleaching (Supplementary Figure S7). This intensity was used to determine the
716 stoichiometry of foci by fitting the first 3 intensity points with a straight line and

717 dividing the intercept by this characteristic intensity. The number of peaks in the
718 Gaussian fits to UvrD was set by running a peak fitting algorithm over the wild type
719 distribution. This number of Gaussians was then used for mutant distributions unless
720 two or more of the Gaussians converged on the same/similar peak value, in which
721 case they were removed. For DnaQ, two peaks were fit as used previously (61). The
722 width of the obtained Gaussian fits was in line with previous measurements (61) and
723 a function of several sources of noise in the challenging live-cell environment,
724 including: fluorophores broad intensity distribution (73) (Supplementary Figure S6);
725 camera noise; cell autofluorescence; and mobility of the protein complexes
726 themselves.

727 GFP and mCherry images were aligned based on the peak of the 2D cross
728 correlation between their respective brightfield images. Colocalisation between foci
729 and the probability of random colocalisation was determined as described previously
730 (65, 107).

731 The microscopic apparent diffusion coefficients (*D*) were determined by fitting a
732 straight line to the first three mean squared displacements (MSD) values constrained
733 through the equivalent localization precision MSD as determined from the intensity
734 (73, 108). *D* distributions were fit by three Gamma distributions as described
735 previously (109–111). Dwell time was calculated as the number of frames that each
736 trajectory was colocalised with the fork position, as determined by the DnaQ foci
737 detected at time zero.

738 **Single-molecule *in vitro* imaging**

739 10 µg/mL mouse anti-GFP (Roche. Cat no. 11814460001) in PBS was incubated on
740 a tunnel slide for 5 min at room temperature, before washing with 100 µL of imaging
741 buffer (20 mM Tris pH 7.8, 5 mM $MgCl_2$, 1 mM DTT). 1 nM of purified mGFP-UvrD in
742 imaging buffer was then flowed onto the slide and incubated at room temperature for
743 5 min before washing with 100 µL of imaging buffer. The ends of the channel were
744 then sealed for imaging. We used a similar single-molecule fluorescence microscope
745 design (107) which enabled Slimfield as for the live cell imaging in order to image the
746 antibody immobilised mGFP-UvrD.

747 **SEC-MALLS**

748 Size Exclusion Chromatography – Multi-Angle Laser Light Scattering (SEC-MALLS)
749 experiments used Wyatt HELEOS-II multi-angle light scattering and rEX refractive
750 index detectors linked to a Shimadzu HPLC system (SPD-20A UV detector, LC20-
751 AD isocratic pump system, DGU-20A3 degasser and SIL-20A autosampler) with a
752 G.E. Superdex S200 10/300 column at a flow rate of 0.5 mL/min in buffer of 20 mM
753 Tris pH 8.3 (at 4degC) 1 mM EDTA, 1 mm EGTA, 1 mM DTT, 200 mM NaCl, 5%
754 glycerol buffer. Data were analysed using Wyatt Astra 7 software. MWs were
755 estimated using the Zimm fit method with degree 1. A value of 0.182 mL/g was used
756 for protein refractive index increment (dn/dc).

757 **Surface plasmon resonance (SPR)**

758 SPR was performed at 25°C on a BIAcore T200 instrument as in (12). Immobilisation
759 of *E. coli* UvrD and Rep was performed onto streptavidin-coated SA sensor chips
760 whilst the indicated concentrations of Tau and UvrB were passed over in 10 mM
761 HEPES pH 7.4, 3 mM EDTA, 150 mM NaCl, 10 mM $MgCl_2$ and 0.05% Tween 20 at
762 20 µl min^{-1}. This buffer differed from that used in the DNA replication assays to
763 minimise non-specific interactions with the surface-immobilised streptavidin. We
764 performed experiments comparable to our previous study (12) in the range ca. 200-
765 4000 nM.

766 **Replication assay**

767 Replication assays were carried out using pPM872 as the template for RNAP blocks
768 (1) or pPM594 (12) for EcoRI E111G blocks. Plasmid pPM872 contains $P_{lacUV5\ 52C}$, a
769 strong promoter in which the first 52 nucleotides of the transcript lack cytosine
770 residues and are then followed by four consecutive cytosines. This enables
771 transcription of $P_{lacUV5\ 52C}$ to be stalled by the omission of CTP. Assays were
772 performed in 40 mM HEPES (pH 8); 10 mM DTT; 10 mM magnesium acetate; 2 mM
773 ATP; 0.2 mM GTP, 0.2 mM UTP; 0.04 mM dNTPs; and 0.1 mg/ml BSA. Reactions
774 (15 µl) contained 2 nM plasmid template, 50 nM DNA polymerase III αεθ complex,
775 25 nM τ clamp loader complex, 160 nM DnaB and DnaC monomers, 1 µM SSB, 80
776 nM β clamp, 30 nM HU, 200 nM DnaG, 300 nM DnaA. Helicases were added as
777 indicated. Rep and UvrD used at 200 nM. *E. coli* RNAP holoenzyme from NEB (1
778 U/µl) was used at 1/3 dilution. Dilution was determined empirically to match RNAP
779 replication inhibition levels from (1). EcoRI E111G was purified as in (112) and used

780 at 200 nM. Reactions were assembled on ice and initiated by addition of DnaA and
781 incubation for 4 min at 37°C, followed by addition of 60 units SmaI (Promega) plus
782 0.4 MBq [α^{32}P] dCTP (222 TBq/mmol). Standard reactions with the helicase present
783 in the initial protein mix were carried out at 37°C for 1 minute and then terminated by
784 addition of 1 µl of 0.5 M EDTA. Delayed helicase addition was carried out by adding
785 Rep/UvrD after 1 minute and incubation for a further minute at 37°C before
786 termination with EDTA. Ethanol precipitated replication products were analysed by
787 denaturing agarose gel electrophoresis (0.7% agarose in 2 mM EDTA, 30 mM NaOH
788 for 400 volt hours, standard run was 16 hours at 25 V), phosphorimaging and
789 autoradiography. 5'-labelled HindIII- digested lambda DNA was used as a marker.
790 Gels were quantified using Quantity One® (Bio-Rad) software. Full-length plasmid
791 replication products were quantified as a proportion of summed blocked products
792 and normalised for length (for EcoRI E111G block), or total lane signal (RNAP
793 block).

794

795
796

797

798
799 **REFERENCES**
800

801 1. M. Hawkins, *et al.*, Direct removal of RNA polymerase barriers to replication by
802 accessory replicative helicases. *Nucleic Acids Res.* **47** (2019).
803 2. R. T. Pomerantz, M. O'Donnell, The replisome uses mRNA as a primer after
804 colliding with RNA polymerase. *Nature* **456**, 762–767 (2008).
805 3. H. Merrikh, C. Machón, W. H. Grainger, A. D. Grossman, P. Soultanas, Co-
806 directional replication-transcription conflicts lead to replication restart. *Nature*
807 **470**, 554–7 (2011).
808 4. A. H. Syeda, J. Atkinson, R. G. Lloyd, P. McGlynn, The balance between
809 recombination enzymes and accessory replicative helicases in facilitating
810 genome duplication. *Genes (Basel).* **7** (2016).
811 5. A. Helmrich, M. Ballarino, L. Tora, Collisions between replication and
812 transcription complexes cause common fragile site instability at the longest
813 human genes. *Mol. Cell* **44**, 966–977 (2011).
814 6. Y. Takeuchi, T. Horiuchi, T. Kobayashi, Transcription-dependent
815 recombination and the role of fork collision in yeast rDNA. *Genes Dev.* **17**,
816 1497–1506 (2003).
817 7. A. L. de Septenville, S. Duigou, H. Boubakri, B. Michel, Replication fork
818 reversal after replication-transcription collision. *PLoS Genet.* **8** (2012).

819 8. C. J. Rudolph, A. L. Upton, A. Stockum, C. A. Nieduszynski, R. G. Lloyd,
820 Avoiding chromosome pathology when replication forks collide. *Nature* **500**,
821 608–611 (2013).
822 9. B. Michel, G. Grompone, M. J. Florès, V. Bidnenko, Multiple pathways process
823 stalled replication forks. *Proc. Natl. Acad. Sci. U. S. A.* **101**, 12783–12788
824 (2004).
825 10. E. V. Mirkin, S. M. Mirkin, Mechanisms of transcription-replication collisions in
826 bacteria. *Mol. Cell. Biol.* **25**, 888–895 (2005).
827 11. P. McGlynn, N. J. Savery, M. S. Dillingham, The conflict between DNA
828 replication and transcription. *Mol. Microbiol.* **85**, 12–20 (2012).
829 12. C. P. Guy, *et al.*, Rep provides a second motor at the replisome to promote
830 duplication of protein-bound DNA. *Mol. Cell* **36**, 654–66 (2009).
831 13. A. H. Syeda, *et al.*, Single-molecule live cell imaging of Rep reveals the
832 dynamic interplay between an accessory replicative helicase and the
833 replisome. *Nucleic Acids Res.* **47**, 6287–6298 (2019).
834 14. P. McGlynn, Linking transcription with DNA repair, damage tolerance, and
835 genome duplication. *Proc. Natl. Acad. Sci. U. S. A.* **107**, 15314–15315 (2010).
836 15. D. Dutta, K. Shatalin, V. Epshtein, M. E. Gottesman, E. Nudler, Linking RNA
837 polymerase backtracking to genome instability in E. coli. *Cell* **146**, 533–543
838 (2011).
839 16. D. Duchi, *et al.*, RNA Polymerase Pausing during Initial Transcription. *Mol. Cell*
840 **63**, 939–950 (2016).
841 17. G. Ghosal, J. Chen, DNA damage tolerance: a double-edged sword guarding
842 the genome. *Transl. Cancer Res.* **2**, 107–129 (2013).
843 18. S. Hamperl, M. J. Bocek, J. C. Saldivar, T. Swigut, K. A. Cimprich,
844 Transcription-Replication Conflict Orientation Modulates R-Loop Levels and
845 Activates Distinct DNA Damage Responses. *Cell* **170**, 774-786.e19 (2017).
846 19. K. Hizume, H. Araki, Replication fork pausing at protein barriers on
847 chromosomes. *FEBS Lett.* **593**, 1449–1458 (2019).
848 20. K. K. Myka, M. E. Gottesman, DksA and DNA double-strand break repair.
849 *Curr. Genet.* **65**, 1297–1300 (2019).
850 21. K. K. Myka, *et al.*, Inhibiting translation elongation can aid genome duplication
851 in Escherichia coli. *Nucleic Acids Res.* **45**, 2571–2584 (2017).
852 22. S. M. Mangiameli, C. N. Merrikh, P. A. Wiggins, H. Merrikh, Transcription leads
853 to pervasive replisome instability in bacteria. *Elife* **6** (2017).
854 23. V. Kamarthapu, *et al.*, ppGpp couples transcription to DNA repair in E. coli.
855 *Science* **352**, 993–996 (2016).
856 24. B. J. Brewer, When polymerases collide: replication and the transcriptional
857 organization of the E. coli chromosome. *Cell* **53**, 679–686 (1988).
858 25. A. Srivatsan, A. Tehranchi, D. M. MacAlpine, J. D. Wang, Co-orientation of
859 replication and transcription preserves genome integrity. *PLoS Genet.* **6**
860 (2010).
861 26. B. Liu, B. M. Alberts, Head-on collision between a DNA replication apparatus
862 and RNA polymerase transcription complex. *Science* **267**, 1131–1137 (1995).
863 27. J. D. Wang, M. B. Berkmen, A. D. Grossman, Genome-wide coorientation of
864 replication and transcription reduces adverse effects on replication in Bacillus
865 subtilis. *Proc. Natl. Acad. Sci. U. S. A.* **104**, 5608–5613 (2007).
866 28. T. S. Sankar, B. D. Wastuwidyaningtyas, Y. Dong, S. A. Lewis, J. D. Wang,
867 The nature of mutations induced by replication–transcription collisions. *Nature*
868 **535**, 178–181 (2016).

869 29. D. Ivanova, *et al.*, Shaping the landscape of the Escherichia coli chromosome:
870 replication-transcription encounters in cells with an ectopic replication origin.
871 *Nucleic Acids Res.* **43**, 7865–7877 (2015).
872 30. A. Helmrich, M. Ballarino, E. Nudler, L. Tora, Transcription-replication
873 encounters, consequences and genomic instability. *Nat. Struct. Mol. Biol.* **20**,
874 412–418 (2013).
875 31. J. G. Brüning, J. L. Howard, P. McGlynn, Accessory replicative helicases and
876 the replication of protein-bound DNA. *J. Mol. Biol.* **426**, 3917–3928 (2014).
877 32. K. R. McDonald, *et al.*, Pfh1 Is an Accessory Replicative Helicase that
878 Interacts with the Replisome to Facilitate Fork Progression and Preserve
879 Genome Integrity. *PLoS Genet.* **12** (2016).
880 33. J. E. Sokoloski, A. G. Kozlov, R. Galletto, T. M. Lohman, Chemo-mechanical
881 pushing of proteins along single-stranded DNA. *Proc. Natl. Acad. Sci. U. S. A.*
882 **113**, 6194–6199 (2016).
883 34. G. D. Schauer, *et al.*, Replisome bypass of a protein-based R-loop block by
884 Pif1. *Proc. Natl. Acad. Sci. U. S. A.* **117**, 30354–30361 (2020).
885 35. M. K. Gupta, *et al.*, Protein-DNA complexes are the primary sources of
886 replication fork pausing in Escherichia coli. *Proc. Natl. Acad. Sci. U. S. A.* **110**,
887 7252–7257 (2013).
888 36. O. Adebali, Y. Y. Chiou, J. Hu, A. Sancar, C. P. Selby, Genome-wide
889 transcription-coupled repair in Escherichia coli is mediated by the Mfd
890 translocase. *Proc. Natl. Acad. Sci. U. S. A.* **114**, E2116–E2125 (2017).
891 37. N. Kang, E. Choi, S. G. Kim, J. Hwang, Inhibitory effect of UvrD and DinG on
892 the replication of ColE1-derived plasmids in Escherichia coli. *Plasmid* **81**, 32–
893 41 (2015).
894 38. V. Epshtein, UvrD helicase: an old dog with a new trick: how one step
895 backward leads to many steps forward. *Bioessays* **37**, 12–19 (2015).
896 39. H. Boubakri, A. L. De Septenville, E. Viguera, B. Michel, The helicases DinG,
897 Rep and UvrD cooperate to promote replication across transcription units in
898 vivo. *EMBO J.* **29**, 145–157 (2010).
899 40. X. Liu, J. X. Seet, Y. Shi, P. R. Bianco, Rep and UvrD Antagonize One Another
900 at Stalled Replication Forks and This Is Exacerbated by SSB. *ACS Omega* **4**,
901 5180–5196 (2019).
902 41. P. R. Caron, S. R. Kushner, L. Grossman, Involvement of helicase II (uvrD
903 gene product) and DNA polymerase I in excision mediated by the uvrABC
904 protein complex. *Proc. Natl. Acad. Sci. U. S. A.* **82**, 4925–4929 (1985).
905 42. B. Van Houten, Nucleotide excision repair in Escherichia coli. *Microbiol. Rev.*
906 **54**, 18–51 (1990).
907 43. A. L. Lu, S. Clark, P. Modrich, Methyl-directed repair of DNA base-pair
908 mismatches in vitro. *Proc. Natl. Acad. Sci. U. S. A.* **80**, 4639–4643 (1983).
909 44. S. W. Matson, A. B. Robertson, The UvrD helicase and its modulation by the
910 mismatch repair protein MutL. *Nucleic Acids Res.* **34**, 4089–4097 (2006).
911 45. L. Manelyte, *et al.*, The unstructured C-terminal extension of UvrD interacts
912 with UvrB, but is dispensable for nucleotide excision repair. *DNA Repair*
913 *(Amst).* **8**, 1300–1310 (2009).
914 46. A. B. Robertson, S. R. Pattishall, E. A. Gibbons, S. W. Matson, MutL-catalyzed
915 ATP hydrolysis is required at a post-UvrD loading step in methyl-directed
916 mismatch repair. *J. Biol. Chem.* **281**, 19949–19959 (2006).
917 47. E. J. Gwynn, *et al.*, The conserved C-terminus of the PcrA/UvrD helicase
918 interacts directly with RNA polymerase. *PLoS One* **8** (2013).

48. K. Sanders, *et al.*, The structure and function of an RNA polymerase interaction domain in the PcrA/UvrD helicase. *Nucleic Acids Res.* **45**, 3875–3887 (2017).
49. V. Epshtein, *et al.*, UvrD facilitates DNA repair by pulling RNA polymerase backwards. *Nature* **505**, 372–377 (2014).
50. B. K. Bharati, *et al.*, Crucial role and mechanism of transcription-coupled DNA repair in bacteria. *Nature* **604**, 152–159 (2022).
51. I. Urrutia-Irazabal, J. R. Ault, F. Sobott, N. J. Savery, M. S. Dillingham, Analysis of the pcra-rna polymerase complex reveals a helicase interaction motif and a role for pcra/uvrd helicase in the suppression of r-loops. *Elife* **10** (2021).
52. B. Martinez, B. K. Bharati, V. Epshtein, E. Nudler, Pervasive Transcription-coupled DNA repair in E. coli. *Nat. Commun.* **13** (2022).
53. N. M. Haines, Y. I. T. Kim, A. J. Smith, N. J. Savery, Stalled transcription complexes promote DNA repair at a distance. *Proc. Natl. Acad. Sci. U. S. A.* **111**, 4037–4042 (2014).
54. A. J. Smith, N. J. Savery, Effects of the bacterial transcription-repair coupling factor during transcription of DNA containing non-bulky lesions. *DNA Repair (Amst).* **7**, 1670–1679 (2008).
55. A. J. Smith, N. J. Savery, RNA polymerase mutants defective in the initiation of transcription-coupled DNA repair. *Nucleic Acids Res.* **33**, 755–764 (2005).
56. J. Atkinson, *et al.*, Stimulation of UvrD helicase by UvrAB. *J. Biol. Chem.* **284**, 9612–9623 (2009).
57. R. P. Wong, N. García-Rodríguez, N. Zilio, M. Hanulová, H. D. Ulrich, Processing of DNA Polymerase-Blocking Lesions during Genome Replication Is Spatially and Temporally Segregated from Replication Forks. *Mol. Cell* **77**, 3-16.e4 (2020).
58. N. K. Maluf, T. M. Lohman, Self-association equilibria of Escherichia coli UvrD helicase studied by analytical ultracentrifugation. *J. Mol. Biol.* **325**, 889–912 (2003).
59. M. Plank, G. H. Wadhams, M. C. Leake, Millisecond timescale slimfield imaging and automated quantification of single fluorescent protein molecules for use in probing complex biological processes. *Integr. Biol.* **1**, 602–612 (2009).
60. A. Badrinarayanan, R. Reyes-Lamothe, S. Uphoff, M. C. Leake, D. J. Sherratt, In vivo architecture and action of bacterial structural maintenance of chromosome proteins. *Science* **338**, 528–31 (2012).
61. R. Reyes-Lamothe, D. J. Sherratt, M. C. Leake, Stoichiometry and architecture of active DNA replication machinery in Escherichia coli. *Science* **328**, 498–501 (2010).
62. T. R. Beattie, *et al.*, Frequent exchange of the DNA polymerase during bacterial chromosome replication. *Elife* **6**, e21763 (2017).
63. R. Reyes-Lamothe, C. Possoz, O. Danilova, D. J. Sherratt, Independent positioning and action of Escherichia coli replisomes in live cells. *Cell* **133**, 90–102 (2008).
64. A. L. Payne-Dwyer, A. H. Syeda, J. W. Shepherd, L. Frame, M. C. Leake, RecA and RecB: probing complexes of DNA repair proteins with mitomycin C in live Escherichia coli with single-molecule sensitivity. *bioRxiv*, 2021.10.04.463068 (2021).
65. I. Llorente-Garcia, *et al.*, Single-molecule in vivo imaging of bacterial

969 respiratory complexes indicates delocalized oxidative phosphorylation.
970 *Biochim. Biophys. Acta* **1837**, 811–24 (2014).
971 66. D. A. Zacharias, J. D. Violin, A. C. Newton, R. Y. Tsien, Partitioning of lipid-
972 modified monomeric GFPs into membrane microdomains of live cells. *Science*
973 **296**, 913–916 (2002).
974 67. A. Oliva, M. Llabrés, J. B. Fariña, Comparative study of protein molecular
975 weights by size-exclusion chromatography and laser-light scattering. *J. Pharm.*
976 *Biomed. Anal.* **25** (2001).
977 68. E. Folta-Stogniew, K. R. Williams, Determination of molecular masses of
978 proteins in solution: Implementation of an HPLC size exclusion
979 chromatography and laser light scattering service in a core laboratory. *J.*
980 *Biomol. Tech.* **10** (1999).
981 69. M. C. Leake, *et al.*, Stoichiometry and turnover in single, functioning
982 membrane protein complexes. *Nature* **443**, 355–358 (2006).
983 70. N. K. Maluf, C. J. Fischer, T. M. Lohman, A Dimer of Escherichia coli UvrD is
984 the active form of the helicase in vitro. *J. Mol. Biol.* **325**, 913–935 (2003).
985 71. H. Yokota, Y. A. Chujo, Y. Harada, Single-molecule imaging of the oligomer
986 formation of the nonhexameric Escherichia coli UvrD helicase. *Biophys. J.* **104**,
987 924–933 (2013).
988 72. H. Yokota, Quantitative and kinetic single-molecule analysis of DNA unwinding
989 by Escherichia coli UvrD helicase. *Biophys. physicobiology* **19**, n/a (2022).
990 73. A. J. M. Wollman, M. C. Leake, Millisecond single-molecule localization
991 microscopy combined with convolution analysis and automated image
992 segmentation to determine protein concentrations in complexly structured,
993 functional cells, one cell at a time. *Faraday Discuss.* **184**, 401–24 (2015).
994 74. A. H. Syeda, *et al.*, Single-molecule live cell imaging of Rep reveals the
995 dynamic interplay between an accessory replicative helicase and the
996 replisome. *Nucleic Acids Res.* **47**, 6287–6298 (2019).
997 75. A. J. Wollman, *et al.*, Transcription factor clusters regulate genes in eukaryotic
998 cells. *Elife* **6** (2017).
999 76. S. Shashkova, A. J. M. Wollman, M. C. Leake, S. Hohmann, The yeast Mig1
1000 transcriptional repressor is dephosphorylated by glucose-dependent and -
1001 independent mechanisms. *FEMS Microbiol. Lett.* **364**, 245 (2017).
1002 77. H. M. Arthur, P. B. Eastlake, Transcriptional control of the uvrD gene of
1003 Escherichia coli. *Gene* **25**, 309–316 (1983).
1004 78. Y. Taniguchi, *et al.*, Quantifying E. coli proteome and transcriptome with
1005 single-molecule sensitivity in single cells. *Science* **329**, 533–8 (2010).
1006 79. G. W. Li, D. Burkhardt, C. Gross, J. S. Weissman, Quantifying absolute protein
1007 synthesis rates reveals principles underlying allocation of cellular resources.
1008 *Cell* **157**, 624–635 (2014).
1009 80. J. Atkinson, M. K. Gupta, P. McGlynn, Interaction of Rep and DnaB on DNA.
1010 *Nucleic Acids Res.* **39**, 1351–1359 (2011).
1011 81. S. V. Rajagopala, *et al.*, The binary protein-protein interaction landscape of
1012 Escherichia coli. *Nat. Biotechnol. 2014 323* **32**, 285–290 (2014).
1013 82. D. K. Orren, C. P. Selby, J. E. Hearst, A. Sancar, Post-incision steps of
1014 nucleotide excision repair in Escherichia coli. Disassembly of the UvrBC-DNA
1015 complex by helicase II and DNA polymerase I. *J. Biol. Chem.* **267**, 780–788
1016 (1992).
1017 83. P. McGlynn, R. G. Lloyd, Modulation of RNA polymerase by (p)ppGpp reveals
1018 a RecG-dependent mechanism for replication fork progression. *Cell* **101**, 35–

1019 45 (2000).
1020 84. Y. N. Zhou, D. J. Jin, The rpoB mutants destabilizing initiation complexes at
1021 stringently controlled promoters behave like “stringent” RNA polymerases in
1022 Escherichia coli. *Proc. Natl. Acad. Sci. U. S. A.* **95**, 2908–2913 (1998).
1023 85. E. A. Campbell, *et al.*, Structural mechanism for rifampicin inhibition of
1024 bacterial rna polymerase. *Cell* **104**, 901–912 (2001).
1025 86. M. Stracy, *et al.*, Live-cell superresolution microscopy reveals the organization
1026 of RNA polymerase in the bacterial nucleoid. *Proc. Natl. Acad. Sci. U. S. A.*
1027 **112**, E4390-9 (2015).
1028 87. K. King, S. J. Benkovic, P. Modrich, Glu-111 is required for activation of the
1029 DNA cleavage center of EcoRI endonuclease. *J. Biol. Chem.* **264**, 11807–
1030 11815 (1989).
1031 88. J. A. Ali, N. K. Maluf, T. M. Lohman, An oligomeric form of E. coli UvrD is
1032 required for optimal helicase activity. *J. Mol. Biol.* **293** (1999).
1033 89. E. Curti, S. J. Smerdon, E. O. Davis, Characterization of the helicase activity
1034 and substrate specificity of Mycobacterium tuberculosis UvrD. *J. Bacteriol.* **189**
1035 (2007).
1036 90. B. Nguyen, Y. Ordabayev, J. E. Sokoloski, E. Weiland, T. M. Lohman, Large
1037 domain movements upon UvrD dimerization and helicase activation. *Proc.*
1038 *Natl. Acad. Sci.* **114**, 12178–12183 (2017).
1039 91. A. Wagner, Robustness against mutations in genetic networks of yeast. *Nat.*
1040 *Genet. 2000 244* **24**, 355–361 (2000).
1041 92. J. Atkinson, *et al.*, Localization of an accessory helicase at the replisome is
1042 critical in sustaining efficient genome duplication. *Nucleic Acids Res.* **39**, 949–
1043 957 (2011).
1044 93. S. C. Massoni, S. J. Sandler, Specificity in suppression of SOS expression by
1045 recA4162 and uvrD303. *DNA Repair (Amst).* **12**, 1072–1080 (2013).
1046 94. K. H. Maslowska, K. Makiela-Dzbenska, I. J. Fijalkowska, The SOS system: A
1047 complex and tightly regulated response to DNA damage. *Environ. Mol.*
1048 *Mutagen.* **60**, 368–384 (2019).
1049 95. R. C. Centore, S. J. Sandler, UvrD limits the number and intensities of RecA-
1050 green fluorescent protein structures in Escherichia coli K-12. *J. Bacteriol.* **189**,
1051 2915–2920 (2007).
1052 96. V. Petrova, *et al.*, Active displacement of RecA filaments by UvrD translocase
1053 activity. *Nucleic Acids Res.* **43**, 4133–4149 (2015).
1054 97. M. M. Cox, Regulation of bacterial RecA protein function. *Crit. Rev. Biochem.*
1055 *Mol. Biol.* **42**, 41–63 (2007).
1056 98. N. Raghunathan, S. Goswami, J. K. Leela, A. Pandiyan, J. Gowrishankar, A
1057 new role for Escherichia coli Dam DNA methylase in prevention of aberrant
1058 chromosomal replication. *Nucleic Acids Res.* **47**, 5698–5711 (2019).
1059 99. H. Yokota, Roles of the C-Terminal Amino Acids of Non-Hexameric Helicases:
1060 Insights from Escherichia coli UvrD. *Int. J. Mol. Sci.* **22**, 1–19 (2021).
1061 100. K. A. Datsenko, B. L. Wanner, One-step inactivation of chromosomal genes in
1062 Escherichia coli K-12 using PCR products. *Proc. Natl. Acad. Sci. U. S. A.* **97**,
1063 6640–6645 (2000).
1064 101. J. G. Brüning, J. A. L. Howard, K. K. Myka, M. S. Dillingham, P. McGlynn, The
1065 2B subdomain of Rep helicase links translocation along DNA with protein
1066 displacement. *Nucleic Acids Res.* **46**, 8917–8925 (2018).
1067 102. J. G. Brüning, J. A. L. Howard, P. McGlynn, Use of streptavidin bound to
1068 biotinylated DNA structures as model substrates for analysis of nucleoprotein

complex disruption by helicases. *Methods* **108**, 48–55 (2016).
103. A. J. M. Wollman, A. H. Syeda, P. McGlynn, M. C. Leake, Single-Molecule Observation of DNA Replication Repair Pathways in E. coli. *Adv. Exp. Med. Biol.* **915**, 5–16 (2016).
104. H. Miller, *et al.*, Superresolution imaging of single DNA molecules using stochastic photoblinking of minor groove and intercalating dyes. *Methods* **88**, 81–8 (2015).
105. M. C. Leake, D. Wilson, B. Bullard, R. M. Simmons, The elasticity of single kettin molecules using a two-bead laser-tweezers assay. *FEBS Lett.* **535**, 55–60 (2003).
106. M. C. Leake, D. Wilson, M. Gautel, R. M. Simmons, The elasticity of single titin molecules using a two-bead optical tweezers assay. *Biophys. J.* **87**, 1112–35 (2004).
107. A. J. M. Wollman, *et al.*, Critical roles for EGFR and EGFR-HER2 clusters in EGF binding of SW620 human carcinoma cells. *J. R. Soc. Interface* **19** (2022).
108. M. C. Leake, *et al.*, Variable stoichiometry of the TatA component of the twin-arginine protein transport system observed by in vivo single-molecule imaging. *Proc. Natl. Acad. Sci. U. S. A.* **105**, 15376–81 (2008).
109. H. Miller, *et al.*, High-Speed Single-Molecule Tracking of CXCL13 in the B-Follicle. *Front. Immunol.* **9**, 1073 (2018).
110. J. Cosgrove, *et al.*, B cell zone reticular cell microenvironments shape CXCL13 gradient formation. *Nat. Commun.* **11** (2020).
111. X. Jin, *et al.*, Membraneless organelles formed by liquid-liquid phase separation increase bacterial fitness. *Sci. Adv.* **7** (2021).
112. S. C. Cheng, R. Kim, K. King, S. H. Kim, P. Modrich, Isolation of gram quantities of EcoRI restriction and modification enzymes from an overproducing strain. *J. Biol. Chem.* **259**, 11571–11575 (1984).
113. S. H. Chung, R. A. Kennedy, Forward-backward non-linear filtering technique for extracting small biological signals from noise. *J. Neurosci. Methods* **40**, 71–86 (1991).

Supplementary Information

Tetrameric UvrD helicase is located at the *E. coli* replisome due to frequent replication blocks

Adam J. M Wollman[1,2,3,], Aisha H. Syeda[1,2], Jamieson A. L. Howard[1,2], Alex Payne-Dwyer[1,2], Andrew Leech[4] , Dominika Warecka[2], Colin Guy[5, 6], Peter McGlynn[2,6], Michelle Hawkins[2] and Mark C. Leake[1,2]

The authors wish it to be known that, in their opinion, the first two authors should be regarded as joint First Authors

[1] School of Physics, Engineering and Technology, University of York, York YO10 5DD, United Kingdom.

[2] Department of Biology, University of York, York YO10 5DD, United Kingdom.

[3] Current address: Biosciences Institute, Newcastle University, NE1 7RU, United Kingdom.

[4] Bioscience Technology Facility, Department of Biology, University of York, York YO10 5DD, United Kingdom

[5] Current address: Covance Laboratories Ltd., Otley Road, Harrogate, HG3 1PY, United Kingdom

[6] Previous address: School of Medical Sciences, Institute of Medical Sciences, University of Aberdeen, Foresterhill, Aberdeen AB25 2ZD, United Kingdom

* To whom correspondence should be addressed. To whom correspondence should be addressed. Tel: +44 (0)1904322697. Email: mark.leake@york.ac.uk

Present Address: School of Physics, Engineering and Technology, and Department of Biology, University of York, York YO10 5DD, United Kingdom

1126 **Supplementary Tables**

1127 **Table S1 Strains used in this study**

Strain	Relevant genotype	Source or derivation
BW25113 derivatives:		
BW25113	*rrnB ΔlacZ4787 hsdR514 Δ(araBAD)567 Δ(rhaBAD)568 rph-1*	(1)
JW2703	*ΔmutS::<kan>*	(1)
JW3786	*ΔuvrD::<kan>*	(1)
JW4019	*ΔuvrA::<kan>*	(1)
MG1655 derivatives:		
TB12	*ΔlacIZYA::<kan>*	
TB28	*ΔlacIZYA*	(2, 3)
TB28 derivatives		
N6577	*ΔlacIZYA Δrep::cat*	(4)
N6661	*ΔlacIZYA::<> Δrep::dhfr* / pAM407 (*uvrD*$^+$ *lacZ*$^+$, a pRC7 derivative)	(4)
N6661	*ΔlacIZYA::<> Δrep::dhfr* / pAM407 (*uvrD*$^+$ *lacZ*$^+$, a pRC7 derivative)	(4)
N6644	*ΔlacIZYA::<> uvrD::dhfr Δrep::cat* / pAM407 (*uvrD*$^+$ *lacZ*$^+$, a pRC7 derivative)	(4)
JGB166	*ΔuvrD* / pKD46	JW3786 transformed with pKD46
AS97	TB28/pKD46	(5)
AS446	*dnaQ-mCherry-<kan>*	
AS448	*dnaQ-mCherry-<>*	(5)
AS512	*mGFP-uvrD-<kan>*	*mGFP-uvrD-<kan>* recombineered into JGB166
AS517	*ΔlacIZYA::<> Δrep::cat mGFP-uvrD-<kan>* / pAM407 (*uvrD*$^+$ *lacZ*$^+$, a pRC7 derivative)	N6661 X P1(AS512)
AS564	*dnaQ-mCherry-<kan> rpoB*35*	PM486 X P1(AS446)
AS571	*dnaQ-mCherry-<> rpoB*35*	AS564 to km^S with pCP20
AS580	*dnaQ-mCherry-<> mGFP-uvrD-<kan>*	AS448 X P1(AS512)
AS582	*dnaQ-mCherry-<> mGFP-uvrD-<kan> rpoB*35*	AS571 X P1(AS512)
AS590	*dnaQ-mCherry-<> mGFP-uvrD-<kan> Δrep::cat*	AS580 X P1(N6577)
AS650	*dnaQ-mCherry-<> mGFP-uvrD-<>*	AS580 to km^S with pCP20
AS656	*dnaQ-mCherry-<> mGFP-uvrD-<> ΔuvrA::<kan>*	AS650 X P1(JW4019)
AS658	*dnaQ-mCherry-<> mGFP-uvrD-<> ΔmutS::<kan>*	AS650 X P1(JW2703)

1128

1129

1130 **Table S2 Plasmids used in this study**

Plasmid	Description	Antibiotic	Reference
pCP20	Yeast Flp recominase expression plasmid	Amp	(6)
pKD46	λ Red recombinase expression plasmid	Amp	(6)
pAS79	pUC18 *mGFP-uvrD-<kan>*	Amp, kan	This study
pAS152	pET14b-mGFP uvrD	Amp	This study

1131
1132

1133 **Table S3 Oligonucleotides used in this study**

Primer	Sequence (5' - 3')
oJGB383	TGAATGATTTTTTAGGCCAAATAAGGTGCGCAGCACCGCATCCGGCAACGCATATGAATATCCTCCTTAG
oJGB417	TACAAGACACGTGCTGAAGTC
oJGB418	TGCTAGTTGAACGCTTCCATC
oMKG71	CGGTGCCCTGAATGAACTGC
oPM319	CTTGTTGGATCAGACCGGAAAATG
oPM320	TGGCAACGCTATCCTTTTGTCA
oPM407	GCGGCAGGCAATGTGGTA
oPM409	CCTTTGAGCGTGTGGTGA
oPM411	CAGCGGCTACAAGCTCGG
oPM187B20	GTCGGATCCTCTAGACAGC(BiodT)CCATGATCACTGGCACTGGTAGAATTCGGC
oPM188B34	AACGTCATAGACGATTACATTGCTACATGGAGC(BiodT)GTCTAGAGGATCCGAC
oAS84	CCCGTCTCGATCTGGTGCAG
oAS85	TTGCTGCAAAAATCGCCCAAG
oAS132	CCCGTCTCGATCTGGTGCAGAAGAAAGGCGGAAGTTGCCTCTGGCGAGCAGGCTGGCTCCGCTGCTGG
oAS133	TTGCTGCAAAAATCGCCCAAGTCGCTATTTTTAGCGCCTTTCACAGGTATCATATGAATATCCTCCTTAG
oAS145	AGGGCGTTGCGCTTCTCCGCCCAACCTATTTTTACGCGGCGGTGCCAATGAGTAAAGGAGAAGAACTT

1134

1135

1136 **Table S4 Cell doubling times of labelled strains.** Values expressed are the means of three
1137 independent replicates, with standard deviation and standard errors indicated.

Strain (Relevant genotype)	LB medium			Minimal medium		
	Mean doubling time (min)	SD (min)	SEM (min)	Mean doubling time (min)	SD (min)	SEM (min)
WT	23.72	1.11	0.64	62.80	17.06	9.85
dnaQ-mCherry	26.85	0.91	0.52	62.22	18.63	10.76
mGFP-uvrD	24.79	0.37	0.22	59.45	1.80	1.04
dnaQ-mCherry mGFP-uvrD	25.27	1.51	0.87	71.03	7.59	4.38
ΔmutS	24.59	0.55	0.32	107.91	13.96	8.06
ΔuvrA	27.99	0.23	0.13	92.25	5.86	3.38
*ΔrpoB*35*	33.98	0.17	0.10	83.11	30.83	17.80
Δrep	24.30	2.03	1.17	62.74	1.20	0.70
dnaQ-mCherry mGFP-uvrD ΔmutS	26.85	0.68	0.39	110.84	34.91	20.16
dnaQ-mCherry mGFP-uvrD ΔuvrA	24.13	0.56	0.33	91.80	5.18	2.99
*dnaQ-mCherry mGFP-uvrD ΔrpoB*35*	32.81	0.70	0.40	99.11	78.68	45.42
dnaQ-mCherry mGFP-uvrD Δrep	26.54	1.90	1.10	62.17	2.98	1.72

1138
1139

1140 **Table S5 Comparison of wild type and labelled UvrD**
1141

Method	Figure	Result
Growth rates	S1	No significant difference
Plasmid loss assays	S2	mGFP-UvrD can rescue cells where UvrD deletion is lethal
In vitro unwinding assay	S3	Nucleoprotein block removal and helicase activity of mGFP-UvrD and biotinylated UvrD was comparable to the wild type
SEC-MALLS	S9	No significant detectable difference in oligomeric state
In vitro replication assay	Fig. 5 and S14	Wild type UvrD and mGFP-UvrD are able to overcome blocks to replication

1142
1143
1144
1145
1146
1147

1148

1149 **Supplementary figures**

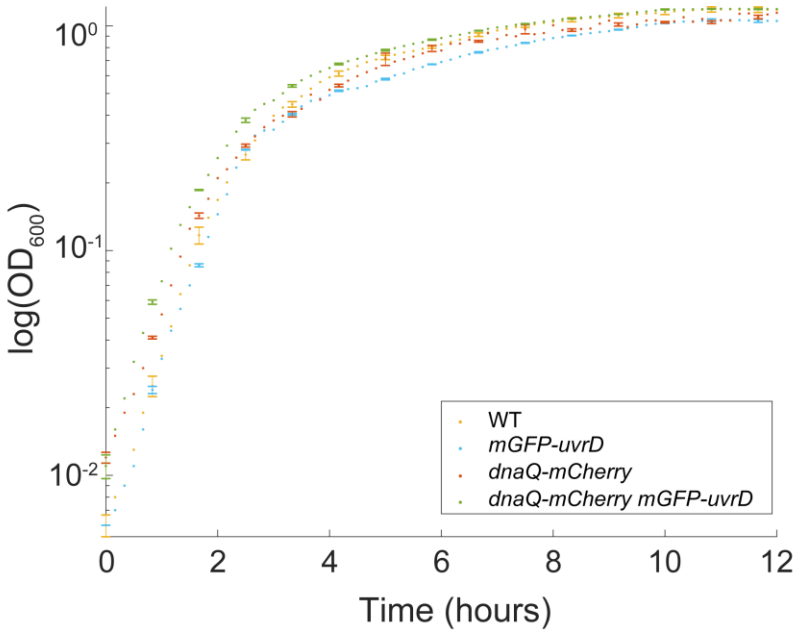

1150

1151

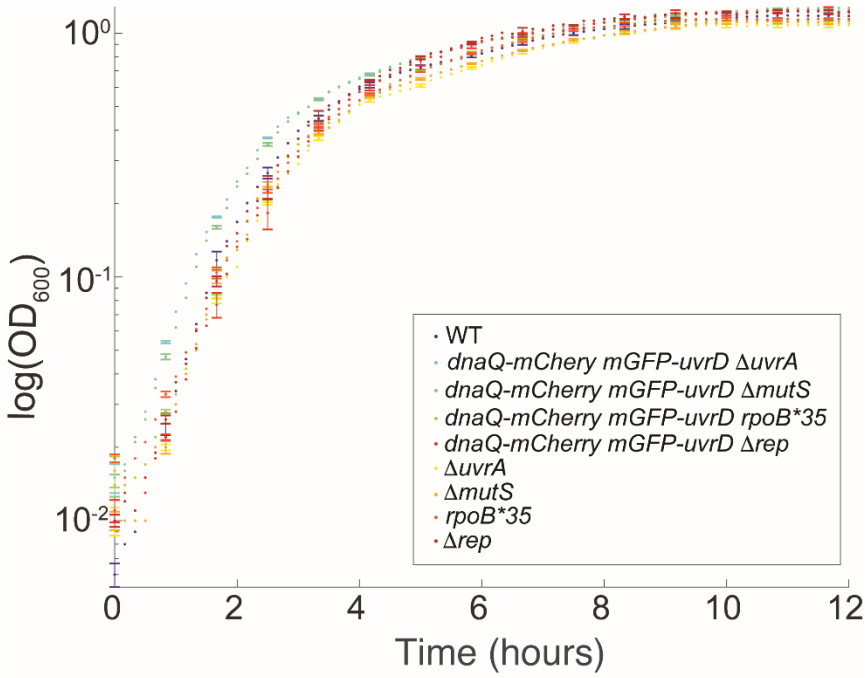

1152

1153 **Supplementary Figure S1. Growth curves in LB medium.** Cultures were grown in LB as
1154 described in the text. The OD_{600} values are plotted on a log scale on the vertical axis with a
1155 linear scale of time in hours on the horizontal axis. The genotypes of the strains are indicated
1156 in boxes within the figures. SD error bars (shown just on every 5th consecutive point for clarity
1157 here), taken from N=3 replicate cultures. Plots in panel A are growth curves of single and dual
1158 labelled wild-type strains, while those in panel B are dual labelled and unlabelled mutant
1159 strains. The unlabelled wild-type strain is included in all panels as a reference.

1160

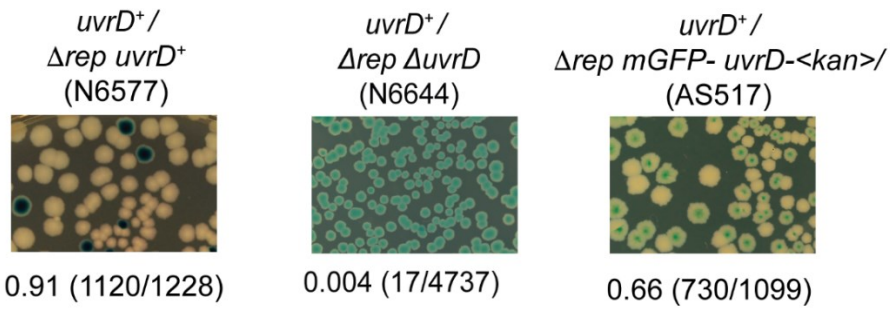

1161

1162 **Supplementary Figure S2: Testing of mGFP-UvrD fusions for retention of function.** We
1163 transformed the strain carrying a chromosomal *mGFP-uvrD* allele with a derivative of pRC7
1164 carrying a wild-type *uvrD* allele (pPM407), which is an unstable low copy plasmid that also
1165 carries the *lacZYA* genes (3). Presence of this plasmid confers blue colour to the colonies on
1166 plates containing Xgal when strains are chromosomally deleted for the *lac* operon. In rapidly
1167 growing cells, cells require either *rep* or *uvrD* for viability, and the loss of both is lethal (4, 7).
1168 Thus, *Δrep* cells with a functional *uvrD* allele are viable and can lose pRC7*uvrD*, evidenced
1169 by appearance of white colonies on LB Xgal IPTG plates, but cells lacking *uvrD* function
1170 cannot survive upon loss of the plasmid resulting in recovery of only blue colonies. The *Δrep*
1171 *mGFP-uvrD* cells produced white colonies on Xgal media, indicating that the *mGFP-uvrD*
1172 fusion is functional.
1173

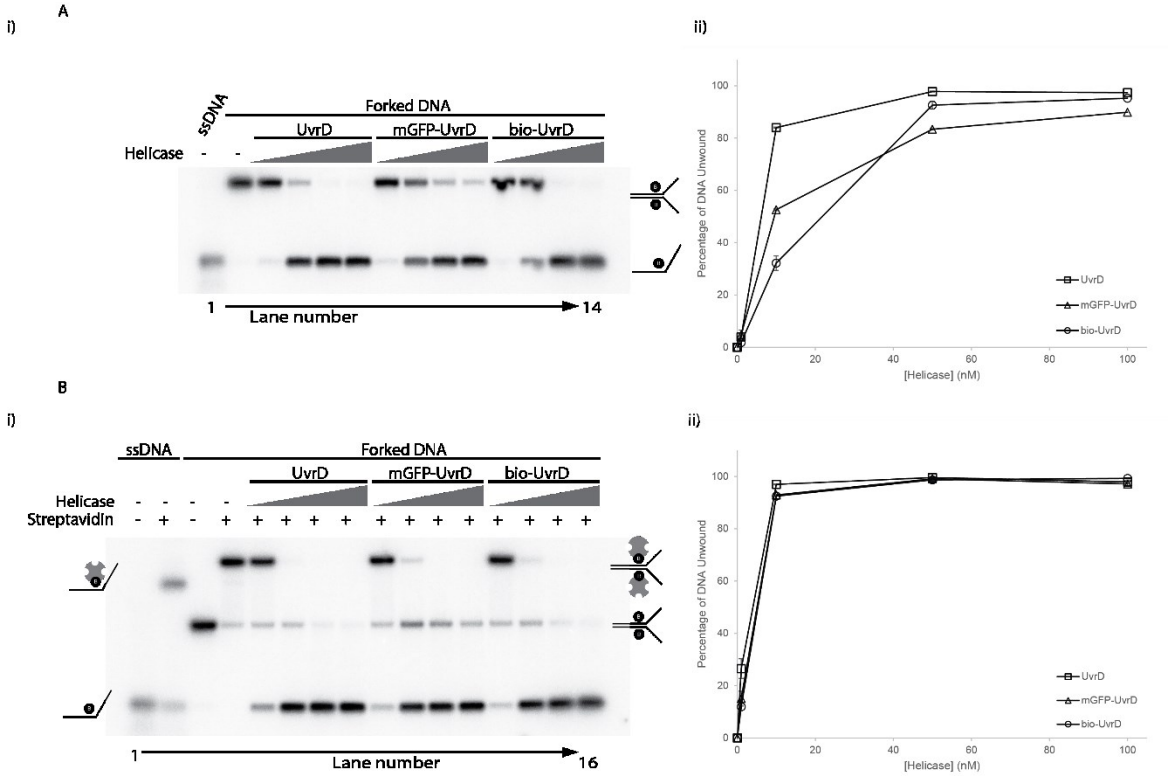

Supplementary Figure S3: mGFP-UvrD fusion is functional *in vitro*. (A)(i) Representative native polyacrylamide TBE gel showing UvrD, mGFP-UvrD and biotinylated-UvrD unwinding of forked DNA containing biotin on both strands within the duplex region (8, 9). Lanes 1-2 contain markers indicating the position of single stranded or forked DNA as indicated. Lanes 3-14 contain the products of unwinding the forked DNA by the indicated helicase at 1, 10, 50 and 100 nM. (ii) Quantification of the unwinding of the forked substrate by the indicated helicases. Data points shown are averages of band intensities (taken from two gels) with standard errors indicated by bars on the points. (B)(i) Representative native polyacrylamide TBE gels showing UvrD, mGFP-UvrD and biotinylated-UvrD unwinding of forked DNA containing biotin on both strands within the duplex region (8, 9). Lanes 1-4 contain markers indicating the position of single stranded or forked DNA +/- streptavidin as indicated. Lanes 5-16 contain the products of unwinding the forked DNA +/- streptavidin by the indicated helicase at 1, 10, 50 and 100 nM. (ii) Quantification of the unwinding of the forked, streptavidin bound substrate by the indicated helicases. Data points shown are averages of band intensities (taken from two gels) with standard errors indicated by bars on the points.

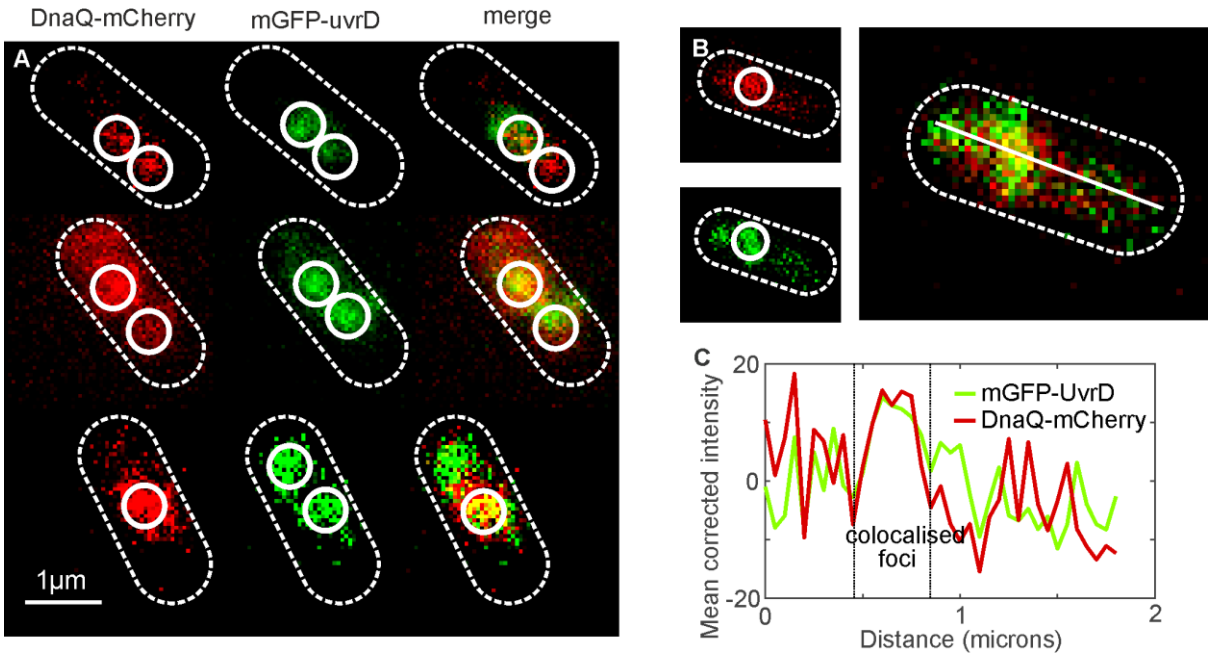

Supplementary Figure S4: Cells typically appear to have two DnaQ foci, but more rarely show just a single DnaQ focus corresponding to two forks separated by less than the optical resolution limit. A. and B. Dual color Slimfield of mGFP-UvrD:DnaQ-mCherry, scale bar 1 micron. Segmented outlines of cell bodies (white dash) and detected foci (white circles) indicated. C. Mean corrected intensity line profile through a colocalized foci in B.

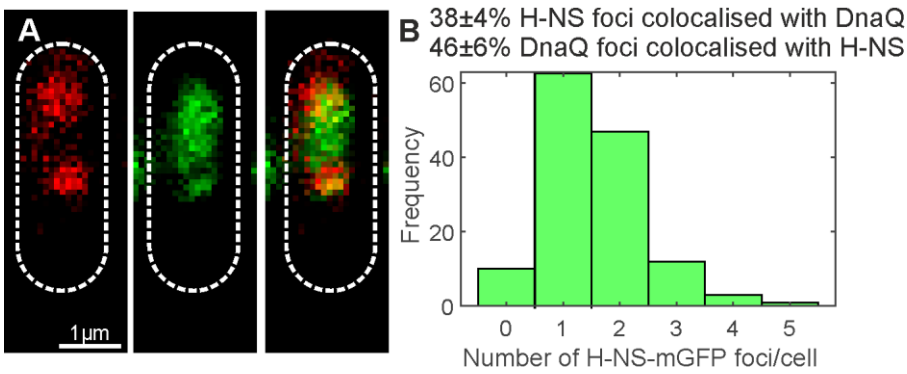

Supplementary Figure S5: H-NS associates with the nucleoid but not specifically with the fork. A. Dual color Slimfield of H-NS-mGFP-:DnaQ-mCherry, scale bar 1 micron. Segmented outlines of cell bodies indicated (white dash). B. Histogram showing the number of H-NS foci detected per cell, SD errors.

1204

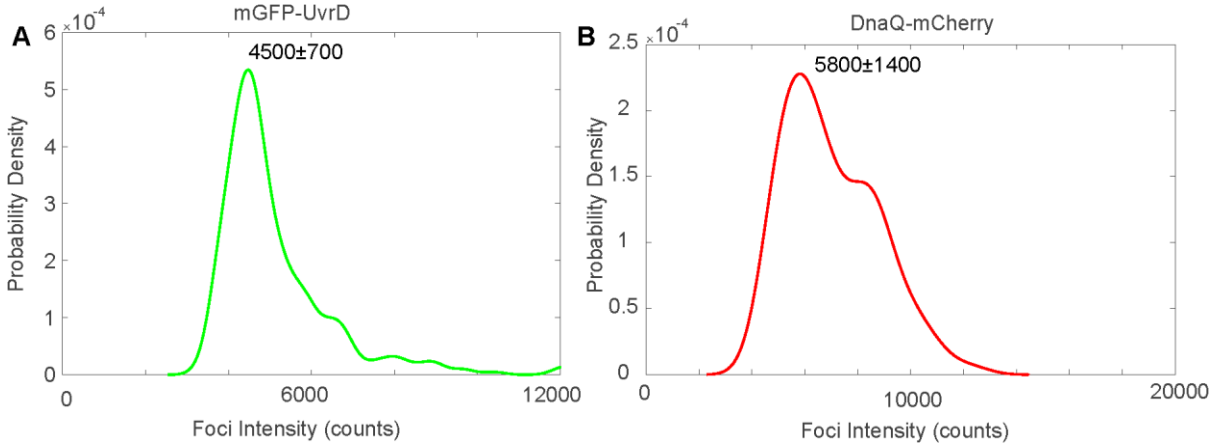

1205

1206 **Supplementary Figure S6: Brightness of single mGFP and mCherry molecules.**
1207 Characteristic intensity distributions rendered as kernel density estimates of single A. mGFP-
1208 UvrD and B. DnaQ-mCherry obtained using Slimfield. Peak±full width at half maximum
1209 indicated. Distributions calculated from the tracked foci intensity distributions from the end of
1210 the photobleach process such that only single fluorophore molecules are detected. Number
1211 of molecules per foci before bleaching is determined by dividing the initial foci intensity by
1212 these values for the equivalent fluorophore.

1213

1214

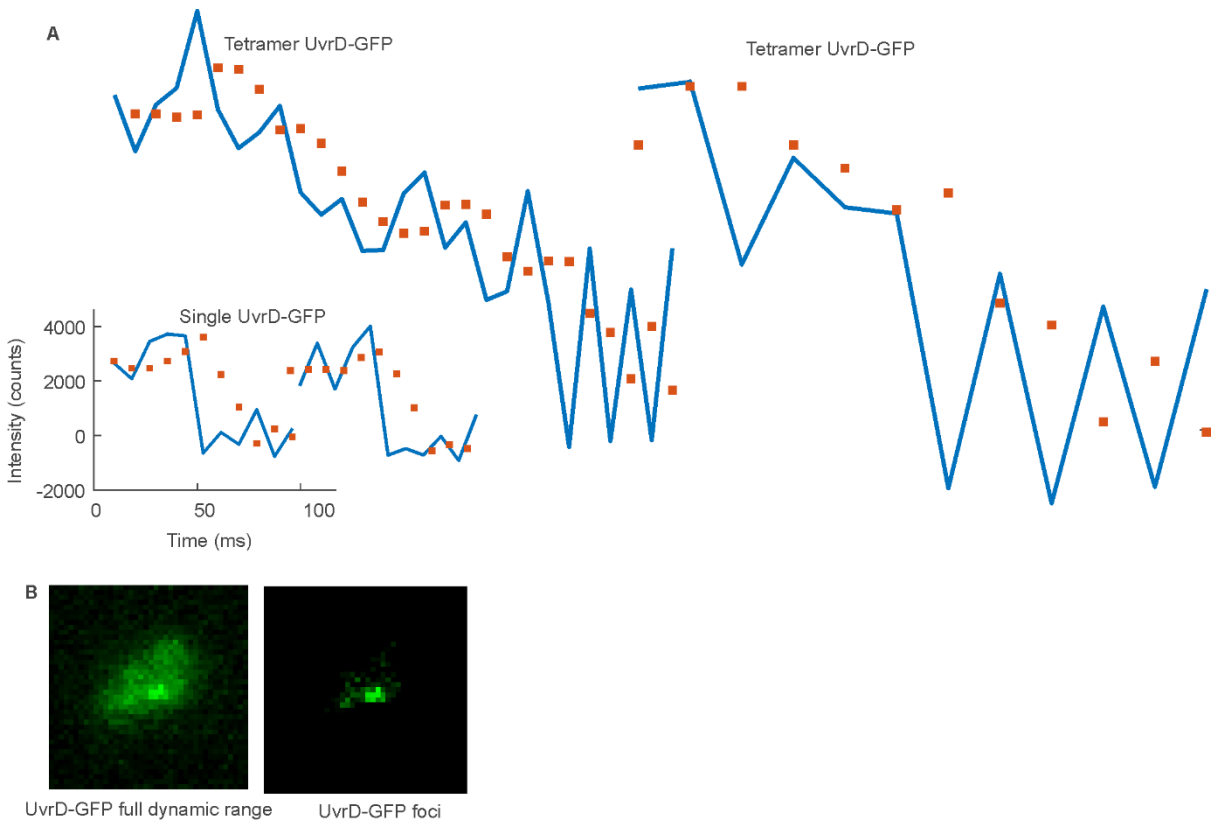

1215
1216
1217 **Supplementary Figure S7: Single-molecule image analysis. A.** Foci intensity as a
1218 function of time for detected UvrD tracks (blue) overlaid by Chung-Kennedy (CK) filtered
1219 intensity (squares). CK filtering is an edge preserving filter allowing noise to be filtered out
1220 while retaining steps.(113) Examples are shown of intensity traces for single UvrD tracks
1221 showing tetramers exhibiting multiple photobleach steps and monomers detected towards
1222 the end of photobleaching. Foci were 'overtracked' beyond the last detected bright frame to
1223 illustrate steps. **B**. UvrD-GFP micrograph showing the full dynamic range (left) and adjusted
1224 to illustrate a foci (right)
1225

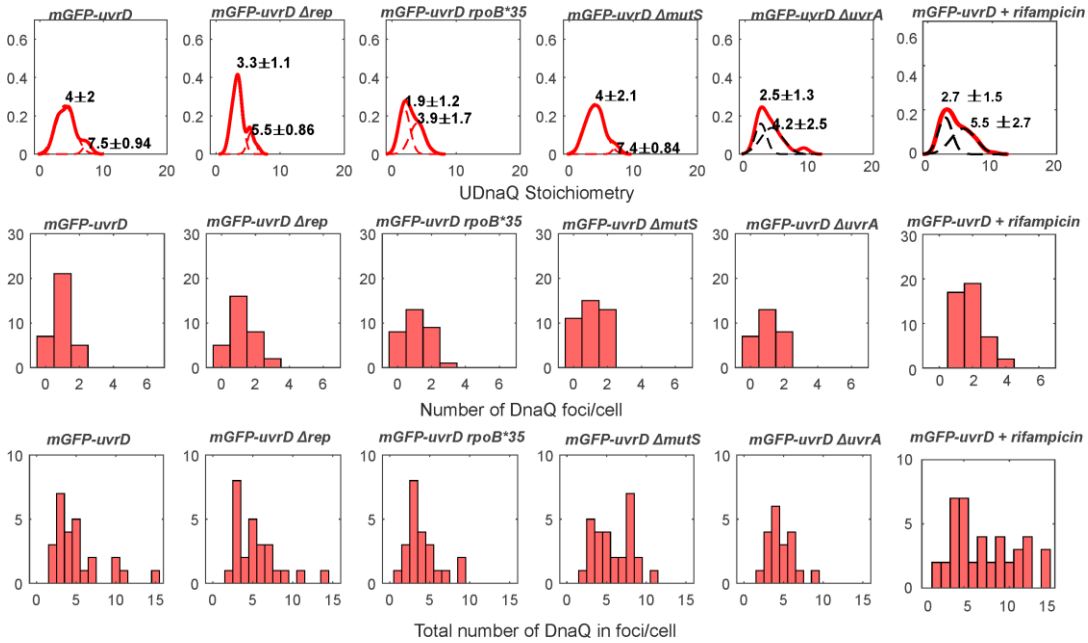

Supplementary Figure S8: DnaQ tracking characterization. Top row: Distribution of DnaQ foci stoichiometry as a kernel density estimate for all strains and conditions (red) with two Gaussian fit overlaid as black dotted lines. Peak ± half width at half maximum shown above. Middle row: Corresponding histogram of number of foci detected per cell. Bottom row: histogram of the total amount of DnaQ in foci per cell. N=30-50 cells per strain or condition.

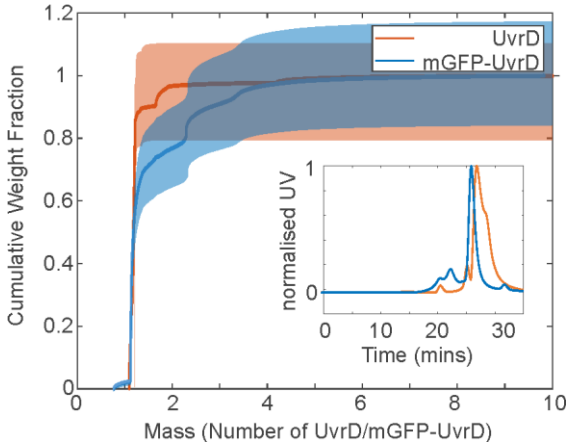

Supplementary Figure S9: SEC-MALLS of UvrD/mGFP UvrD Size Exclusion Chromatography - Multi-Angle Laser Light Scattering (SEC-MALLS) of 4 μM UvrD (red) and mGFP-UvrD (blue) cumulative weight fraction as a function of molar mass in number of UvrD/mGFP-UvrD, shading indicates 16% indicative error bounds consistent with sensitivity error measurements reported from polydispersed heterogenous samples using SEC-MALLS (68), and consistent with our own estimation of sensitivity using our SEC-MALLS system. Inset shows the normalised UV absorbance as a function of elution time through the column with the monomer peaks indicated.

1247

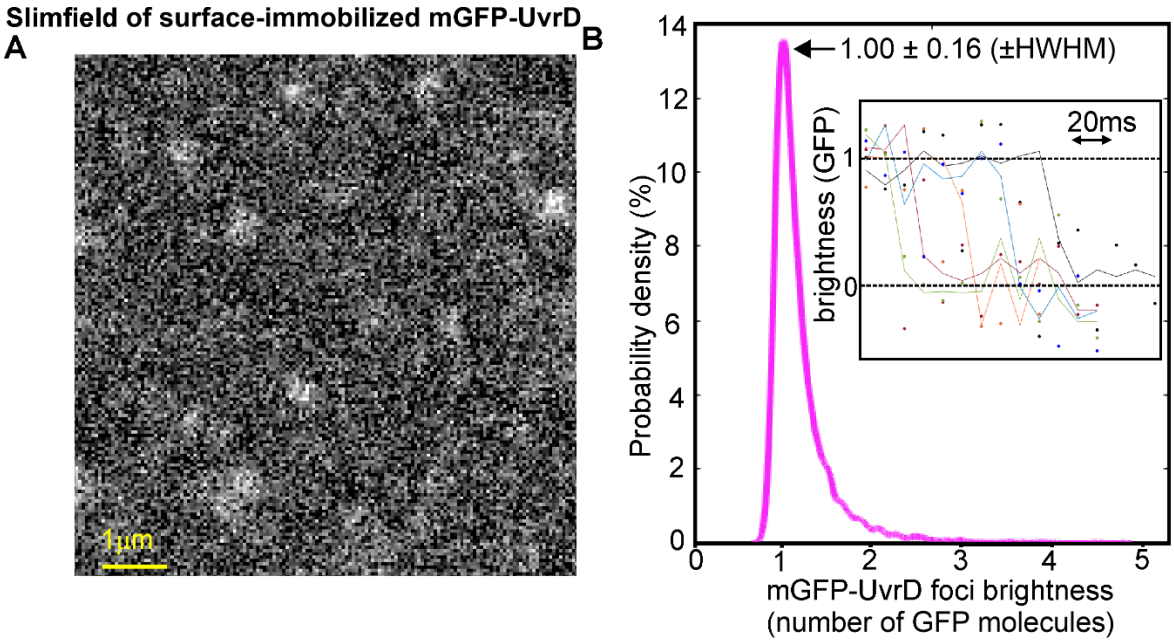

1248
1249
1250 **Supplementary Figure S9: Single-molecule microscopy of purified mGFP-UvrD**
1251 **indicates most foci contain monomeric mGFP-UvrD.** A. Representative Slimfield of
1252 surface-immobilized mGFP-UvrD. B. Automated single-particle tracking output for mGFP-
1253 UvrD showing probability distribution for mGFP-UvrD foci brightness normalized by the
1254 single-molecule dye brightness, peak (±HWHM) corresponding to 1 molecule indicated
1255 (arrow) for n=7,384 foci. *Inset*: example overlaid stepwise photobleach traces for four
1256 different mGFP-UvrD foci indicating a consistent single-molecule step to zero brightness
1257 whose size is comparable to the measured modal brightness across all foci (dots: raw data,
1258 lines: Chung-Kennedy edge-preserving filter output).

1259
1260

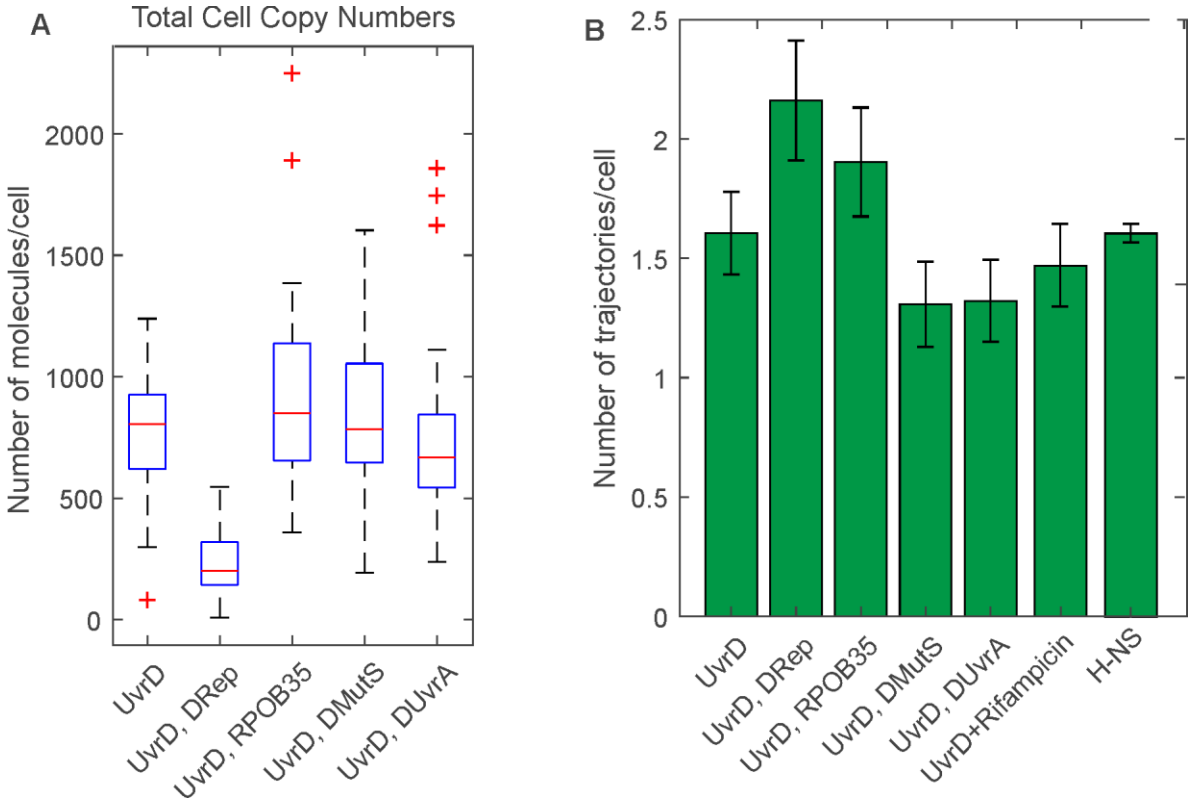

Supplementary Figure S10: A. Boxplot of the total number of mGFP-UvrD molecules per cell, estimated by numerical integration of the whole cell fluorescence. Median is shown as red line, bottom and top of the blue box mark the 25th and 75th percentiles and whiskers extend to the most extreme points not considered outliers (2.7 standard deviations covering 99.3% of normally distributed data) with outliers beyond this shown as red +. N=30 cells per strain. B Number of trajectories per cell used in the stoichiometry determination

1271

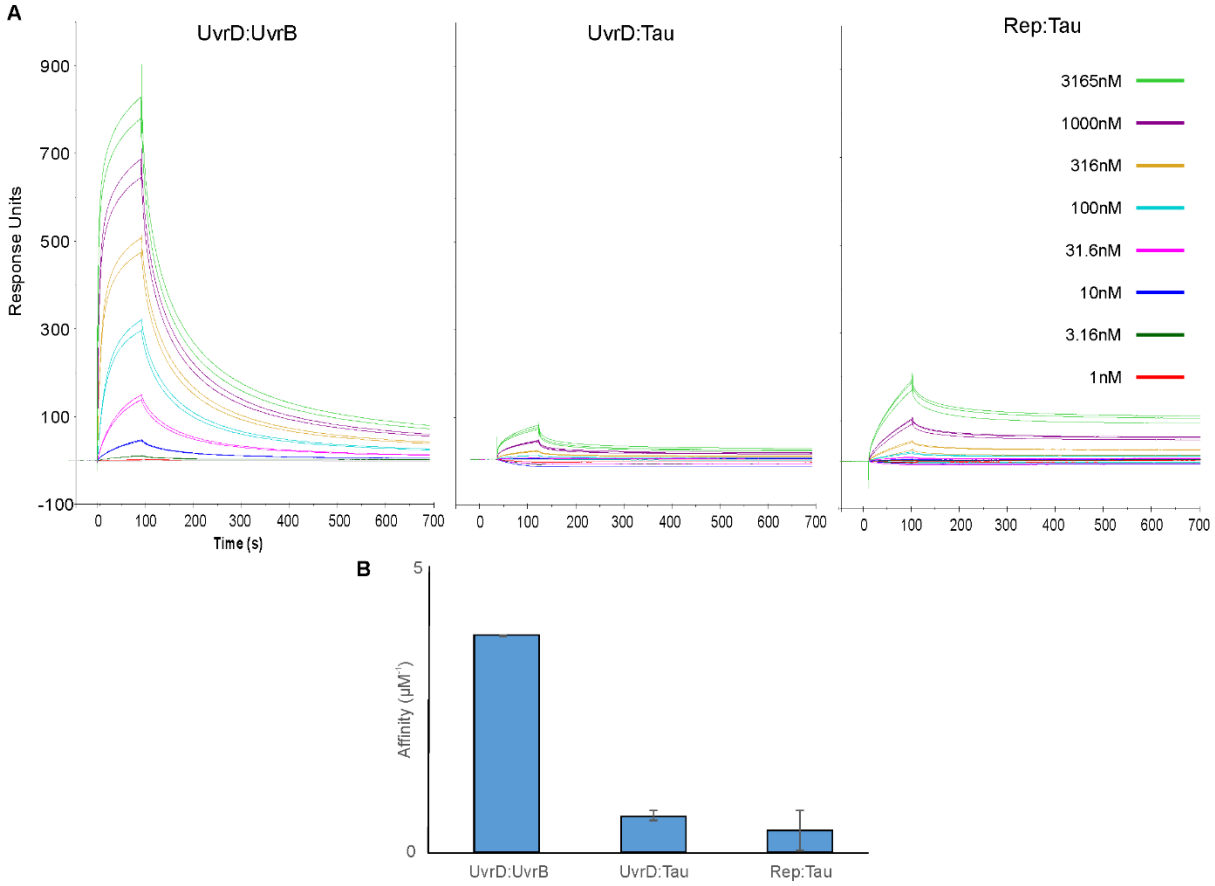

1272

1273 **Supplementary Figure S11: Surface plasmon resonance measurements of helicase**
1274 **interactions with Tau** A. Titration response sensorgrams for UvrD:UvrB, UvrD:Tau and
1275 Rep:Tau with indicated analyte concentrations. B. Binding affinity plotted as association
1276 constant (K_a, uM-1) for the UvrD:UvrB, UvrD:Tau and Rep:Tau interactions assuming a single
1277 sites binding model. The respective dissociation constants K_d are 231 nM, 1.4 μM and
1278 2.3 μM.SD error bars.

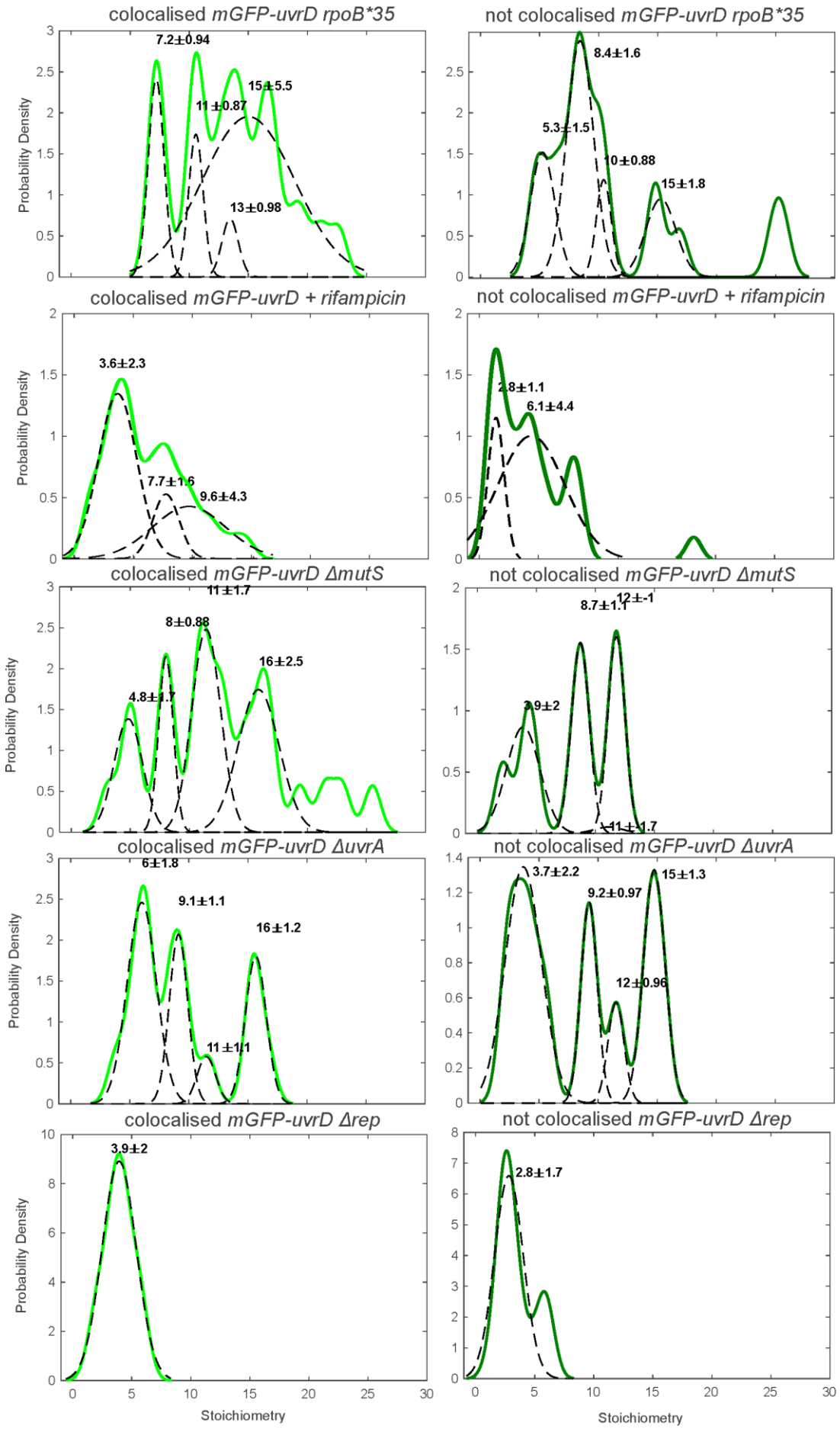
colocalised mGFP-uvrD rpoB*35
7.2±0.94
11±0.87
15±5.5
13±0.98
not colocalised mGFP-uvrD rpoB*35
8.4±1.6
5.3±1.5
10±0.88
15±1.8
colocalised mGFP-uvrD + rifampicin
3.6±2.3
7.7±1.6
9.6±4.3
not colocalised mGFP-uvrD + rifampicin
2.8±1.1
6.1±4.4
colocalised mGFP-uvrD ΔmutS
11±1.7
8±0.88
16±2.5
4.8±1.7
not colocalised mGFP-uvrD ΔmutS
8.7±1.1
12±-1
3.9±2
11±1.7
colocalised mGFP-uvrD ΔuvrA
6±1.8
9.1±1.1
16±1.2
11±1.1
not colocalised mGFP-uvrD ΔuvrA
3.7±2.2
9.2±0.97
15±1.3
12±0.96
colocalised mGFP-uvrD Δrep
3.9±2
not colocalised mGFP-uvrD Δrep
2.8±1.7
Probability Density
Stoichiometry

1279

1280 **Supplementary Figure S12:** Perturbed UvrD stoichiometry. The distribution of UvrD foci
1281 stoichiometry rendered as a kernel density estimate for foci colocalised (Left) and non-
1282 colocalised (Right) with DnaQ foci. Distributions were fitted with multiple Gaussian fits (black
1283 dotted lines) with the peak value ± half width at half maximum indicated above each peak.
1284

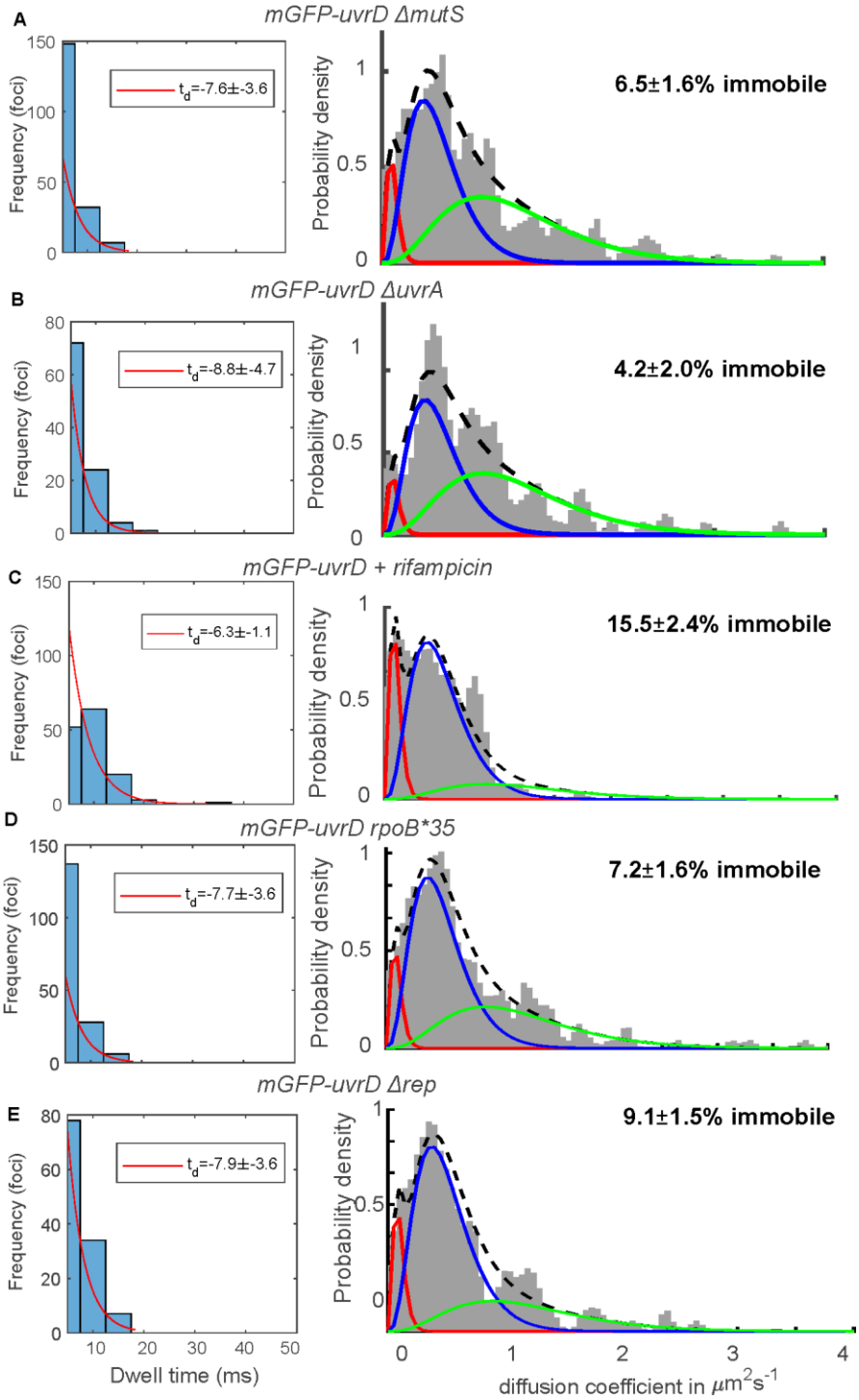

Supplementary Figure S13: UvrD perturbed dynamics. A-E Left, distribution of time UvrD and DnaQ foci were colocalised (blue) fit with an exponential (red) to yield a characteristic dwell time. Right, distribution of microscopic diffusion coefficients of UvrD foci (grey) fitted with a three-state gamma distribution model containing a relatively immobile population with D = 0.1 μm^2/s (red), a transiently immobile population, D = 0.5 μm^2/s (blue) and a mobile population, D=1.2 μm^2/s (green). Errors represent 95% confidence intervals. N~300 foci/condition.

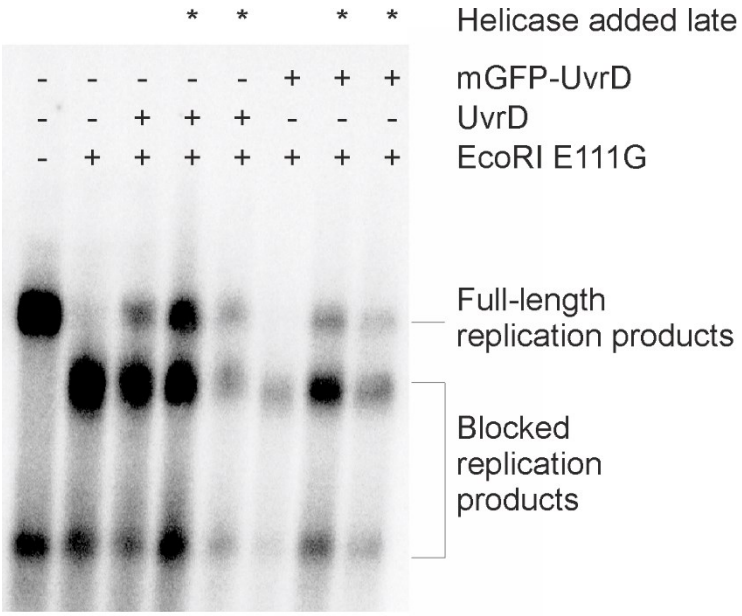

Supplementary Figure S14: In vitro replication assay using mGFP-UvrD. Denaturing agarose gel of replication products formed from pPM872 (1) in the absence and presence of EcoRI E111G block, mGFP-UvrD and UvrD added pre- and post-collision (*) as indicated.

Supplementary references

1. Baba,T., Ara,T., Hasegawa,M., Takai,Y., Okumura,Y., Baba,M., Datsenko,K.A., Tomita,M., Wanner,B.L. and Mori,H. (2006) Construction of Escherichia coli K-12 in-frame, single-gene knockout mutants: the Keio collection. *Mol. Syst. Biol.*, **2**, 2006.0008.
2. Bachmann,B.J. (1996) Derivations and genotypes of some mutant derivatives of Escherichia coli K-12. . In Neidhardt,F.C., Curtiss III,R., Ingraham,J.L., Lin,E.C.C., Low,K.B., Magasanik,B., Reznikoff,W.S., Riley,M., Schaechter,M., Umbarger,H.E. (eds), *Escherichia coli and Salmonella cellular and molecular biology*. ASM Press, Washington, DC, pp. 2460–2488.
3. Bernhardt,T.G. and de Boer,P.A.J. (2004) Screening for synthetic lethal mutants in Escherichia coli and identification of EnvC (YibP) as a periplasmic septal ring factor with murein hydrolase activity. *Mol. Microbiol.*, **52**, 1255–1269.
4. Guy,C.P., Atkinson,J., Gupta,M.K., Mahdi,A.A., Gwynn,E.J., Rudolph,C.J., Moon,P.B., van Knippenberg,I.C., Cadman,C.J., Dillingham,M.S., *et al.* (2009) Rep provides a second motor at the replisome to promote duplication of protein-bound DNA. *Mol. Cell*, **36**, 654–666.
5. Syeda,A.H., Wollman,A.J.M., Hargreaves,A.L., Howard,J.A.L., Brüning,J.-G., McGlynn,P. and Leake,M.C. (2019) Single-molecule live cell imaging of Rep reveals the dynamic interplay between an accessory replicative helicase and the replisome. *Nucleic Acids Res.*, **47**, 6287–6298.
6. Datsenko,K.A. and Wanner,B.L. (2000) One-step inactivation of chromosomal genes in *Escherichia coli* K-12 using PCR products. *Proc. Natl. Acad. Sci. USA*, **97**, 6640–6645.
7. Boubakri,H., de Septenville,A.L., Viguera,E. and Michel,B. (2010) The helicases DinG, Rep and UvrD cooperate to promote replication across transcription units in vivo. *EMBO J.*, **29**, 145–157.
8. Brüning,J.-G., Howard,J.A.L. and McGlynn,P. (2016) Use of streptavidin bound to biotinylated DNA structures as model substrates for analysis of nucleoprotein complex disruption by helicases. *Methods*, **108**, 48–55.
9. Brüning,J.-G., Howard,J.A.L., Myka,K.K., Dillingham,M.S. and McGlynn,P. (2018) The 2B subdomain of Rep helicase links translocation along DNA with protein displacement. *Nucleic Acids Res.*, **46**, 8917–8925.